

Mind the Modality Gap: Towards a Remote Sensing Vision-Language Model via Cross-modal Alignment

Angelos Zavras, Dimitrios Michail, Begüm Demir, Ioannis Papoutsis

Abstract—Deep Learning (DL) is undergoing a paradigm shift with the emergence of foundation models, aptly named by their crucial, yet incomplete nature. In this work, we focus on Contrastive Language-Image Pre-training (CLIP), an open-vocabulary foundation model, which achieves high accuracy across many image classification tasks and is often competitive with a fully supervised baseline without being explicitly trained. Nevertheless, there are still domains where zero-shot CLIP performance is far from optimal, such as Remote Sensing (RS) and medical imagery. These domains do not only exhibit fundamentally different distributions compared to natural images, but also commonly rely on complementary modalities, beyond RGB, to derive meaningful insights. To this end, we propose a methodology for the purpose of aligning distinct RS imagery modalities with the visual and textual modalities of CLIP. Our two-stage procedure, comprises of robust fine-tuning CLIP in order to deal with the distribution shift, accompanied by the cross-modal alignment of a RS modality encoder, in an effort to extend the zero-shot capabilities of CLIP. We ultimately demonstrate our method on the tasks of RS imagery classification and cross-modal retrieval. We empirically show that both robust fine-tuning and cross-modal alignment translate to significant performance gains, across several RS benchmark datasets. Notably, these enhancements are achieved without the reliance on textual descriptions, without introducing any task-specific parameters, without training from scratch and without catastrophic forgetting.

Index Terms—Remote sensing, foundation model, vision-language model, multi-modal learning, cross-modal alignment, cross-modal retrieval, cross-modal distillation, satellite representation learning.

I. INTRODUCTION

TRADITIONAL earth surface mapping and monitoring, has been constrained to expensive and time-consuming, methods (e.g field surveys), with data acquired over lengthy intervals. For real-time global and regional mapping, these methods are quite inefficient and impractical. EO is not new, but historically, the utilization of EO data was constrained to the specialized scientific community, due to the limitations posed by the satellite infrastructure available and the accessibility of data and analytical tools. However, recent advancements in these areas, coupled with breakthroughs in data processing techniques, have democratized the use of EO data, enabling the widespread use of this information at scale. Because of the massive volume of data transmitted every day

from many sensors monitoring earth, Remote Sensing (RS) provides fertile ground for the application of modern machine learning (ML) algorithms. Notably, as of today, Europe’s Copernicus satellite constellation alone is producing more than 25 terabytes of satellite data every day, which as a matter of fact outstrips our capacity to extract meaningful information.

DL models for RS imagery classification are typically either trained from scratch using supervised learning methods [1] or fine-tuned for the downstream task, after self-supervised pre-training [2] or transfer learning from another task [3]. Unfortunately, those models are capable of simply enumerating numeric classes behind the scenes, completely disregarding the semantic information encapsulated within each class label. As a result, these models are exceptionally fragile, designed to excel only within the narrow classification space for which they were specifically trained. This discrepancy, is of great interest in the EO community since various nomenclatures and classification schemes are used, while researchers and practitioners continue to explore new schemes and refine existing ones to enhance the understanding of Earth’s surface and its dynamic behavior. These schemes play a crucial role in classifying and interpreting the data, enabling effective analysis and information extraction, depending on the objectives of the study, available data, and the desired level of detail and accuracy required for the analysis.

In contrast to typical image classifiers, open-vocabulary models are not constrained to a fixed classification space and are able to perform any image classification task, using textual descriptions of the class names. On the other hand, foundation models [4], commonly trained via self-supervision at scale, on large amounts of unlabeled data obtained through web-crawling approaches, are large and versatile deep learning models that can be adapted to a wide range of downstream tasks. Open-vocabulary foundation models, represent a powerful combination of large-scale pre-training and the ability to handle words outside of a fixed vocabulary. These models have gathered considerable attention due to their exceptional performance and ability to generalize across different domains and are particularly useful in scenarios where the textual input may include domain-specific terms.

In this work, we investigate OpenAI’s Contrastive Language-Image Pre-Training (CLIP) model, one of the so-called open-vocabulary foundation models, which is able to comprehend concepts of both visual and textual modalities and predict the most relevant text description without being explicitly optimized for the task. Nevertheless, there are still domains where zero-shot CLIP performance is far from optimal, such as RS and medical imagery. Satellite scene classification, in

A. Zavras is with Orion Lab, National Observatory of Athens, National Technical University of Athens and Harokopio University of Athens

D. Michail is with Harokopio University of Athens

B. Demir is with Technische Universität Berlin

I. Papoutsis is with Orion Lab, National Observatory of Athens and National Technical University of Athens

particular, is one of the few tasks presented by the CLIP authors, where zero-shot CLIP significantly under-performs on the EuroSAT dataset, resulting in the biggest delta (37,1%) among all tasks assessed, when compared to a fully supervised ResNet50 baseline model. To this end, we identify three major gaps for the task of satellite scene classification which we address in this work. The first gap regards the distribution shift [5], i.e. a change in the underlying data distribution that can occur when the data used during training, significantly differs from the data the model encounters when deployed, leading to significant performance degradation. Satellite imagery does not only demonstrate a fundamentally different distribution compared to natural images, but it also poses unique challenges in terms of spatial resolution, atmospheric conditions, and varying perspectives due to different orbits, which can significantly impact the performance of computer vision models. The second gap arises from the information constraint induced by relying solely on the RGB modality. Satellite imagery commonly exploit complementary modalities, beyond RGB, to derive meaningful insights. These modalities include multi-spectral, hyper-spectral and radar data, as well as byproducts of those modalities such as InSAR [6] data. Leveraging these diverse modalities grants us with critical and complementary information that contribute to a deeper understanding of our planet. The third gap, pertains to the scarcity of datasets containing pairs of satellite imagery and corresponding textual descriptions. Typically used RS image-text paired datasets [7]–[10], are limited to aerial and Very High-Resolution (VHR) commercial satellite imagery. There are two interrelated drawbacks in these datasets. First, they do not rely on free and open-access data, such as the Copernicus Sentinel satellite constellation data. Second, the spatial resolution of these datasets, which directly relates to the level of detail that can be retrieved from a scene, leads to a different underlying data distribution compared to non-commercial satellite data. Both factors limit their usability in downstream applications.

In order to address these gaps, we propose a novel methodology comprised of two consecutive stages, working towards cross-modal alignment of RS imagery modalities in the context of CLIP. Our study is based on OpenAI’s CLIP collection of pre-trained image-text models. For the first step, we define a patching process to robustly fine-tune CLIP using RS data RGB composites, in order to deal with the aforementioned distribution shift without impacting CLIP zero-shot performance on natural image classification tasks. As for the second step, we extend CLIP’s zero-shot capabilities by cross-modal aligning a pre-trained RS encoder with the visual and textual modalities of CLIP. We ultimately demonstrate our method on the task of RS imagery classification. We empirically show that both robust fine-tuning and cross-modal alignment translate to notable performance gains, over several RS imagery classification benchmark datasets.

Our main contributions can be summarized as follows:

- We propose a novel methodology for cross-modal alignment of RS imagery modalities in the context of CLIP, without the reliance on textual descriptions, without introducing any task-specific parameters, without training

from scratch and without catastrophic forgetting.

- We evaluate the generalization of both patched and aligned models, and provide an extensive benchmark on a series of prominent RS imagery datasets for the task of RS imagery classification and cross-modal retrieval.
- We set the baseline for cross-modal retrieval and text-based zero-shot tasks, in comparison to a representative CLIP supported task (i.e ImageNet) proving that our final Vision-Language model (VLM) extends CLIP pre-training.
- We present an improved CLIP model that now attains good zero-shot performance on RS imagery classification and cross-modal retrieval tasks. This enhancement is achieved by effectively capturing the semantic content of RS, transcending nomenclature limitations and leveraging complementary information, beyond RGB, utilizing available RS imagery modalities. We have made our code implementation and weights for all experiments publicly available, aiming to facilitate the development of novel applications based on RS data.

II. RELATED WORK

A. Contrastive Language-Image Pre-training

Recent developments in the multi-modal contrastive learning era have significantly enhanced the capabilities of CLIP-like models. Such models are notorious for their ability to extract rich visual and textual features, with exceptional discriminative competence [11]–[13] and are suitable for a variety of downstream tasks, such as image classification [14], action recognition [15], semantic segmentation [16], text-guided image generation [17], image and video captioning [18]–[20]. Lately, such models have been also utilized either in part or in their entirety, as versatile building blocks for the next generation of foundation models [21]–[24]. It is evident that CLIP due to its large scale pre-training, as well as its proven efficacy on a wide range of downstream tasks and applications, emerges as an advantageous frontier in the ongoing quest towards foundation models for EO.

LAION-AI with OpenCLIP [25], the open-source implementation of OpenAI’s CLIP [14], has demonstrated impressive results. They managed to replicate OpenAI’s proprietary pre-training dataset [26] and subsequently trained and published several models [27], using various architectures, on a variety of data sources and compute budgets, ranging from small to large-scale experiments. Recent advancements in the context of CLIP pre-training have showcased remarkable achievements along the axes of pre-train data filtering [28]–[30], model architecture [31] and computational efficiency [32]–[34], leading to substantial improvements and eventually establishing new standards within the era of pre-trained CLIP models. These advancements, formulate an imperative demand for an extensive set of benchmarking experiments, aiming to assess the ability of those newly released pre-trained CLIP models to facilitate novel applications, in the context of RS.

B. Domain Specialized CLIP Models

Data is regarded as the cornerstone for foundation model training and CLIP is no exception. Existing CLIP models are

trained on large amounts of web-crawled data, to encode general knowledge, without emphasizing on specialized domains such as RS and medical imagery, which as a matter of fact demonstrate fundamentally different distributions compared to natural images encountered during pre-training.

Several efforts have been made to overcome this phenomenon and adapt CLIP aiming to yield a robust foundation model with proficient expertise in specialized domains. Unlike natural image-text datasets, which can easily reach billion-scale [26], [28], specialized datasets hold a relatively limited scale due to their innate demand for highly targeted knowledge. The medical imaging community, for instance, has witnessed a significant surge in contributions of CLIP-centered studies [35]–[38]. They commonly encompass biomedical image-caption pairs, collected and filtered from open-access research papers [39]–[42], medical reports [43]–[45] and social media platforms [46], [47]. On the contrary, the RS domain lags behind, in terms of CLIP-oriented developments, primarily due to the in-domain image-text paired data scarcity. To this end, recent developments predominantly revolve around the exploitation of existing limited extent RS datasets and the data efficient adaptation of CLIP models to the problem at hand.

Arutiunian et al. [48] fine-tuned CLIP by leveraging three small existing RS image captioning datasets and demonstrated their results on retrieval-related tasks. Czerkawski et al. [49] highlighted that in zero-shot setting, CLIP exhibits difficulty detecting cloud-free images and mitigated this limitation through a cost-effective training stage consisting of a few hundred optimization steps of a single linear layer on top of CLIP image encodings, demonstrating improved performance and transferability across various sensor types and spectral bands. Singha et al. [50] proposed APLeNet, an image-conditioned prompt learning strategy for few-shot RS image generalization using CLIP models. Their approach focuses on multi-scale feature learning and disentangles visual style and content primitives for domain generalization tasks in RS, outperforming zero-shot CLIP in several RS benchmark datasets. Liu et al. [51] presented RemoteCLIP, a RS domain specialized CLIP model, fine-tuned using existing remote sensing image captioning datasets, extended using heterogeneous satellite and UAV imagery annotations (e.g bounding boxes and masks) after turning them into image-caption pairs, achieving remarkable results across various datasets and downstream tasks. Zhang et al. [52] presented RS5M, a 5 million RS image captioning dataset, obtained by filtering publicly available image-text paired datasets and captioning label-only RS datasets with pre-trained VLM, with the purpose of fine-tuning CLIP. They experimented with full fine-tuning and several Parameter-Efficient Fine-Tuning methods and ultimately demonstrated their final model GeoRSCLIP, on zero-shot classification, cross-modal image-text retrieval and semantic localization tasks in comparison to state-of-the-art RS-tailored CLIP models. Yuan et al. [53] introduced a Parameter-Efficient Transfer Learning (PETL) [54] method for RS Image-Text Retrieval, leveraging a pre-trained CLIP model along a multi-modal adapter and a Hybrid Multi-modal Contrastive learning objective, outperforming traditional methods and showcasing a

drastic reduction in training costs compared to full fine-tuning. Mo et al. [55] proposed S-CLIP, a semi-supervised learning method for fine-tuning CLIP that utilizes additional unpaired images by employing pseudo-labeling strategies specifically designed for contrastive learning, significantly enhancing fine-tuning results using fewer image-text pairs than typically required. Bhattacharya et al. [56] proposed C-SAW, a self-supervised prompt learning technique which incorporates a reconstruction task for better image generalization in RS applications. During fine-tuning, they kept the CLIP backbone frozen and introduced a small set of projectors for both CLIP encoders to train contrastively using C-SAW. Dhakal et al. [57] introduced a novel weakly supervised method for creating maps based on free-form textual descriptions, termed zero-shot mapping. They utilized a contrastive learning framework named Sat2Cap, trained on paired overhead and ground-level images, to predict CLIP embeddings of ground-level scenery from satellite images. They managed to map a wide variety of attributes without text-labeled data, overcoming the limitations of previous models that could only map pre-defined attributes. Similarly, Mall et al. [58] addressed the scarcity of textual descriptions, by training contrastively an image encoder that maps RGB satellite imagery to the same representation space of a frozen CLIP image encoder, using a large amount of paired internet images and RGB satellite composites. They managed to yield state-of-the-art results across numerous downstream tasks and indicated that leveraging a large number of ground-satellite image pairs without accompanying text is more beneficial than fine-tuning on small datasets, in a supervised manner.

It is evident that the main focus in tailoring CLIP for RS revolves around overcoming the scarcity of in-domain image-text paired data. Efforts span from leveraging limited-scale and synthetic datasets for fine-tuning to innovative data-efficient and self-supervised strategies, all aimed at optimizing CLIP for RS. Our work stands out by exploiting existing labeled RS imagery data to deal with the RS domain distribution shift, without introducing any task-specific parameters to the pre-trained CLIP models and without catastrophic forgetting.

C. Multi-modal CLIP-inspired models in Remote Sensing

Multi-modal learning in the RS domain [59] has evolved significantly, marking a transition from traditional single-source data analysis to the integration of diverse RS data types, such as optical imagery and radar, to attain a more accurate and holistic understanding of the Earth. Over time, advancements in machine learning and data fusion [60] techniques have led to sophisticated models that can handle the complexity and variability of multi-modal RS data [61]–[63]. Recently, the introduction of CLIP [14] has significantly influenced the development of RS models capable of seamlessly integrating various modalities, demonstrating an intuitive and versatile approach that extends well beyond the initial image-text framework. This advancement has opened up new possibilities for more intuitive and semantically rich analyses of RS imagery, allowing models to complement and correlate the same Earth features as being observed by different sensors, demonstrating

the growing potential of multi-modal learning in capturing the intricate features of our planet.

In this context, Allen et al. [64] pre-trained a ViT-based CLIP model using three different RS imagery modalities (Sentinel-2 RGB optical and Sentinel-1 SAR radar amplitude and interferometric coherence), across five AOIs covering a small percentage of Earth’s total landmass. The model consists of three separate single channel ViT-based input encoders, operating on whatever channel was randomly selected for each modality, during pre-training, aiming to create a shared embedding space between all three modalities, while similarity is measured for each pair of modalities and then averaged. Klemmer et al. [65] demonstrated SatCLIP, a global, geographic location encoder that learns general-purpose, implicit representations using globally available satellite imagery, pre-trained by matching satellite images and their respective coordinates using the CLIP objective. Along the same lines, Cepeda et al. [66] introduced GeoCLIP, a CLIP-inspired Image-to-GPS retrieval approach for worldwide geo-localization. Unlike SatCLIP, GeoCLIP leverages a pre-trained CLIP image encoder and enforces alignment with the corresponding GPS locations. Using hierarchical learning and random Fourier features, GeoCLIP demonstrated impressive effectiveness in limited-data settings and potential application in a plethora of downstream tasks. Khanal et al. [67] proposed GeoCLAP, a contrastive-learning framework for the task of soundscape mapping based on the relationship between sound and the visual characteristics of geographic locations. They leveraged a CLIP-based model to encode three types of data: geo-tagged audio recordings, textual descriptions of audio, and overhead images of their capture locations. As a result they enabled a unified embedding space, for all three modalities, that can predict the most probable sounds at any given geographic location, outperforming previous state-of-the-art models.

A fundamental notion that distinguishes our work from related research, is the cross-modal alignment of complementary RS imagery modalities, beyond RGB, within the shared embedding space of CLIP, leveraging its large-scale pre-training. Our endeavors focus on aligning a multi-spectral Sentinel-2 encoder with the RGB-image and text encoders of CLIP, providing a blueprint for the cross-modal alignment of more RS imagery modalities and ultimately enabling a rich set of cross-modal retrieval and text-based zero-shot downstream tasks.

III. METHOD

Let $D = \{(\mathcal{I}_{SAT}^1, y_1), \dots, (\mathcal{I}_{SAT}^n, y_n)\}$ be a labeled RS imagery archive consisting of n image-label pairs, where $(\mathcal{I}_{SAT}^n, y_n)$ is the n th image-label pair in the archive. Each image \mathcal{I}_{SAT}^i has a corresponding RGB composite image $\mathcal{I}_{RGB}^i \subset \mathcal{I}_{SAT}^i$, produced using a dedicated function $T_{RGB}()$ depending on the RS modality of \mathcal{I}_{SAT}^i . Given the set of RS imagery \mathcal{I}_{SAT} and the corresponding set of RGB composites \mathcal{I}_{RGB} , along with associated labels y , we aim to learn a shared embedding space E , by utilizing RGB composites and labels as anchors, in order to effectively align these modalities. The objective is to find a mapping $f : \mathcal{I}_{SAT} \cup \mathcal{I}_{RGB} \cup y \rightarrow E$

such that for each triplet $(\mathcal{I}_{SAT}^i, \mathcal{I}_{RGB}^i, y_i)$, the embeddings $f(\mathcal{I}_{SAT}^i)$, $f(\mathcal{I}_{RGB}^i)$, and $f(y_i)$ are closely aligned in E . The final embedding space E enables multi-modal downstream tasks by facilitating the association between RS imagery modalities, RGB images, and text through learned representations.

To this end, we take a two-stage approach, explicitly defined in Algorithm 1. The first step addresses the distribution shift in satellite imagery by robustly fine-tuning the CLIP image encoder. Subsequently, in the second stage the satellite multi-spectral modality embeddings are aligned with the RGB image and text embeddings, i.e. Sentinel-2 multi-spectral imagery to RGB composites and text. The resulting embedding space, effectively associates pairs of modalities, enabling a plethora of cross-modal retrieval and text-based zero-shot downstream tasks.

A. First Stage: Patching CLIP by interpolating weights

Large pre-trained models such as CLIP [14], ALIGN [69] and BASIC [70] have demonstrated unprecedented robustness to a plethora of challenging distribution shifts. However, there are still settings where their zero-shot performance is far from optimal. To this end, Patching with Interpolation (PAINT) [68] has emerged as a method that substantially improves accuracy under distribution shift, while maintaining high performance on the target distribution. PAINT employs a two-step procedure, which consists of fine-tuning the model and then linearly interpolating between the weights of the model before and after fine-tuning. This approach enables the expansion of the set of tasks on which models achieve high accuracy, without introducing any task-specific parameters, without re-training them from scratch, and without catastrophic forgetting [71].

In order to deal with the distribution shift between natural images and satellite imagery we initially robustly fine-tune CLIP, as shown in Fig. 1, following the patching protocol described in Ilharco et al. [68]. Eventually, we end up with a refined embedding space, thus providing a solid foundation to facilitate the satellite cross-modal alignment stage. Given an open-vocabulary model, i.e. CLIP, with weights W_{zs} , we fine-tune W_{zs} on training data from a patching task D_{patch} , aiming to produce weights W_{ft} that achieve high accuracy on D_{patch} , without decreasing the performance on supported tasks D_{supp} , where performance is already adequate. Thus, a mixing coefficient $\alpha \in [0, 1]$ is determined via held-out validation sets for D_{supp} and D_{patch} , in order to linearly interpolate W_{zs} and W_{ft} and produce $W_{patch} = (1 - \alpha) \times W_{zs} + \alpha \times W_{ft}$. Essentially, W_{zs} , W_{ft} and W_{patch} are the weights of a CLIP image encoder. Instead of introducing a learnable classification layer, Ilharco et al. [68] used the frozen output of CLIP’s text, as the output layer of the image encoder in order to map image features to the space of classes, during the course of fine-tuning.

B. Second Stage: Aligning RS imagery modalities with natural images and text

The main objective of contrastive representation learning is to create a shared embedding space where similar sample pairs are close together and dissimilar pairs are far apart.

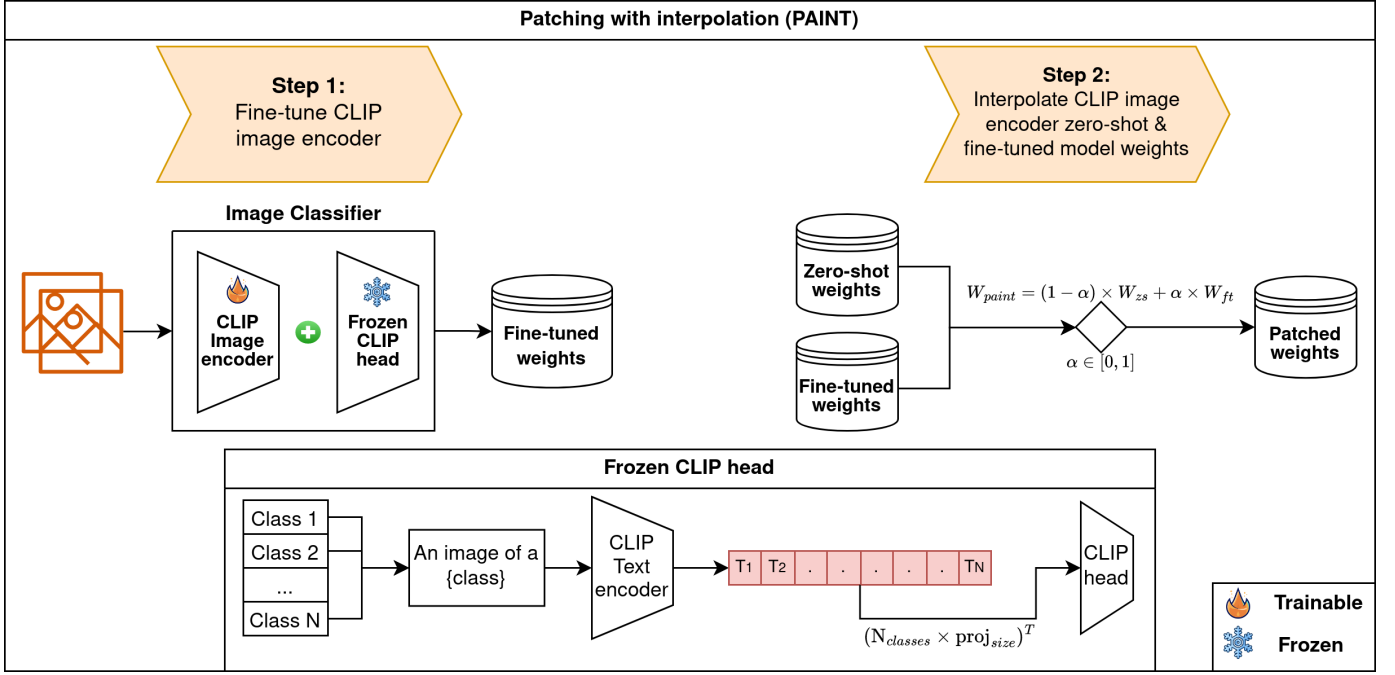


Fig. 1: Patching with interpolation (PAINT) [68] is utilized in the first stage of our method, in order to deal with the underlying distribution shift of the satellite data, without compromising the performance of CLIP on supported tasks, i.e tasks where performance is already adequate.

This technique can be applied in both supervised and unsupervised learning scenarios, with particular effectiveness in self-supervised learning. Contrastive learning also allows for aligning specific pairs of modalities, such as images and text or audio and text. By using pairs of related and unrelated examples, contrastive learning enables the alignment of these modalities in a joint embedding space. However, it's important to note that the resulting embeddings are specific to the aligned modalities and may not directly transfer to other modalities. For instance, embeddings obtained from aligning image and audio modalities may not be directly applicable to text-based tasks. CLIP leverages the aligned (image-text) embedding space for the zero-shot classification task. Given a list of textual descriptions generated using the candidate classes, an input image is classified based on their similarity in the embedding space. Extending the zero-shot classification to other modalities usually requires additional training using paired text data, e.g (audio, text).

In the cross-modal alignment stage (as shown in Fig. 2), we leverage the patched CLIP image encoder $\mathcal{M}_{\text{patched}}$, used in the first stage, as the teacher network, and a pre-trained satellite modality encoder \mathcal{M}_{sat} as the student network. To effectively align these two networks, we adopt a straightforward approach grounded in the assumption that diverse modalities associated with the same sample should yield similar embeddings within the shared CLIP embedding space. The process involves a pair of modalities \mathcal{I}_{RGB} and \mathcal{I}_{SAT} corresponding to RGB composites and some other satellite modality. For a given image $x_i \in \mathcal{I}_{RGB}$ and its corresponding sample $\tilde{x}_i \in \mathcal{I}_{SAT}$ from the two modalities, we obtain their respective embeddings $E_i = \mathcal{M}_{\text{patched}}(x_i)$ and $\tilde{E}_i = \mathcal{M}_{\text{sat}}(\tilde{x}_i)$. In cases where the

embedding dimensions of E_i and \tilde{E}_i differ, we introduce a linear projection head for the student network \mathcal{M}_{sat} to ensure matching output embedding sizes.

Inspired by the knowledge distillation [72] loss function, as well as previous distillation works [73]–[76], the student is guided to mimic the teacher's visual and textual embeddings via a joint objective function formulated as the linear combination of cross-entropy \mathcal{L}_{CE} and mean squared error loss \mathcal{L}_{MSE} .

$$\mathcal{L}_{I,M} = \mathcal{L}_{MSE}(E_i, \tilde{E}_i) + \lambda \times \mathcal{L}_{CE}(y_{\text{pred}}, y_{\text{true}}) \quad (1)$$

\mathcal{L}_{CE} is determined by labeled data supervision using the frozen output of CLIP's text encoder as an anchor to map image features to the space of classes, while \mathcal{L}_{MSE} encourages the student to imitate the output embeddings of the teacher, in contrast to the softened class scores in the case of the original knowledge distillation loss.

IV. EXPERIMENTS

A. Datasets

We utilize three benchmark datasets for RS image classification, featuring a total of 5 different nomenclatures. These datasets vary in terms of the input satellite data specifications, but more importantly, they have adopted different labeling nomenclatures to describe the semantic content of the satellite images (see fig.3).

BigEarthNet [77] comprises of 590326 atmospherically corrected Sentinel-2 (S2-L2A) patches acquired between June 2017 and May 2018 over 10 European countries. The dataset is designed for multi-label LULC scene classification, each image patch is a section of i) 120×120 pixels for 10m

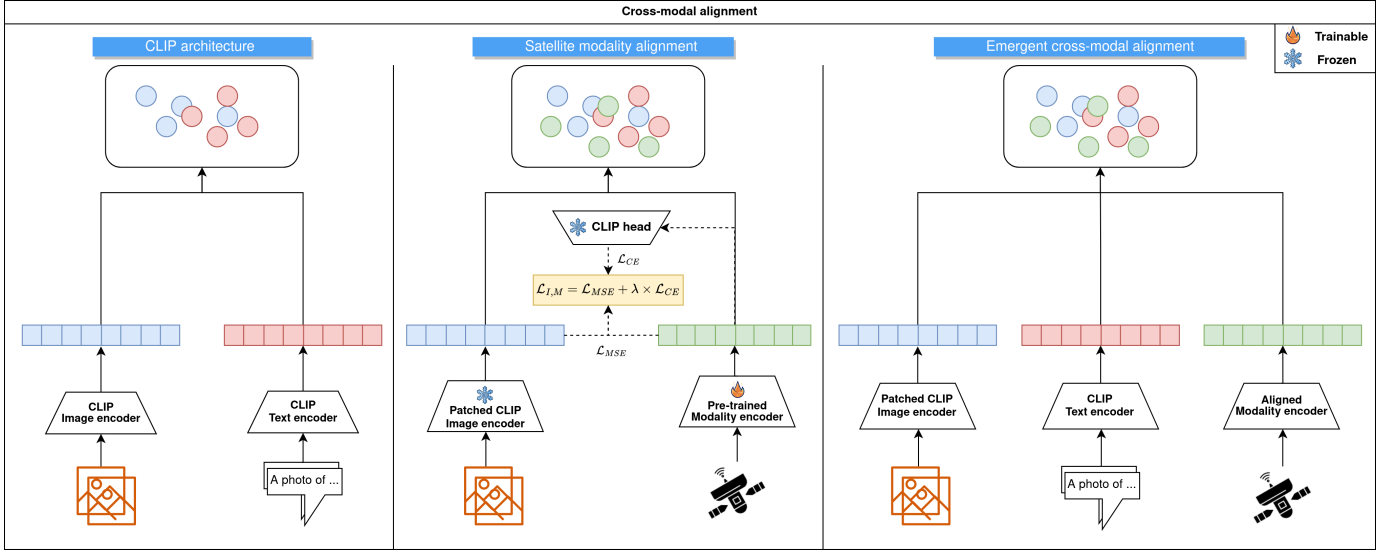


Fig. 2: The second stage of our method concerns the cross-modal alignment of a satellite modality encoder. The image depicts: (A) the standard CLIP [14] architecture, (B) our satellite modality alignment with the visual and textual modalities of CLIP and (C) the emergent cross-modal alignment.

TABLE I: Synopsis of the fundamental traits of the satellite datasets employed during the course of our experiments.

Dataset	# of samples	Patch size	Modalities	Spatial Coverage	Temporal Coverage	Atmospherically Corrected	Nomenclature
BigEarthNet	590.326	120×120	S1, S2	Europe	Single season per patch	True	CORINE LULC L1, L2, L3
SEN12MS	541.986	256×256	S1, S2	Global	Single season per patch	False	MODIS IGBP, LCCS
EuroSAT	27.000	64×64	RGB, S2	Europe	Single season per patch	False	10 generic LULC classes

bands; ii) 60×60 pixels for 20m bands; and iii) 20×20 pixels for 60m bands and is annotated with multiple land-cover classes sourced from the CORINE Land Cover (CLC) database of the year 2018 [78]. The annotations are based on the detailed CORINE Level-3 class nomenclature, supplemented by an alternative 19-class LULC nomenclature [79] introduced by the authors, specifically for use in the machine-learning domain. The dataset has been ultimately expanded to include Synthetic Aperture Radar Sentinel-1 (S1) patches, resulting in Sentinel-1 and Sentinel-2 patch pairs [1]. Consequently, the term BigEarthNet now encompasses both the BigEarthNet-S1 and BigEarthNet-S2 datasets.

EuroSAT [80] consists of 27000 single-date non-atmospherically corrected Sentinel-2 (S2-L1C) patches, distributed all over Europe, of size 64×64 pixels. The dataset is designed for multi-class LULC classification tasks and features a simple 10-class nomenclature. All 27000 patches have been manually checked.

SEN12MS [81] comprises of 180662 patch triplets that include Sentinel-1 dual-polarization SAR data, non-atmospherically corrected Sentinel-2 (S2-L1C) multi-spectral images and MODIS-derived land cover maps. These patches are of size 256×256 pixels and are geographically distributed across Earth’s inhabited continents while encompassing all four meteorological seasons. The dataset is designed for multi-label, multi-class LULC scene classification and semantic segmentation tasks. The four-band MODIS land cover patches have been created using 2016 data, at an upsampled pixel spacing of 10m. The first band contains land cover follow-

ing the International Geosphere-Biosphere Programme (IGBP) classification scheme [82], while the remaining bands contain the Land Cover Classification System (LCCS) land cover, land use and hydrology layers [83]. The authors have ultimately redesigned their dataset [84], featuring a simplified IGBP scheme [85] for single-label and multi-label scene classification tasks, in order to ensure comparability with other land cover schemes and mitigate, to some extent, the class imbalance of their dataset.

B. Experimental Setup

Tasks. Following Ilharco et al. [68], tasks are categorized as patching and supported tasks. Out of the diverse set of image classification tasks from Radford et al. [14], we use ImageNet [86] as a representative supported task and BigEarthNet-S2 [1] as a representative patching task for satellite scene classification.

Prompts. For each downstream dataset, we use a set of pre-defined prompts for each class, which we collected from prior works. We primarily use the prompts assembled by Radford et al. [14] for each downstream dataset, so that we provide a fair comparison of our results. In the case of satellite imagery datasets that were not present in the CLIP collection of downstream datasets (e.g. BigEarthNet), we use the alternative set of prompts proposed by Zhai et al. [87] for satellite datasets. Our approach follows the methodology introduced by Radford et al. [14], commonly referred to as “prompt ensembling” and includes the generation of multiple

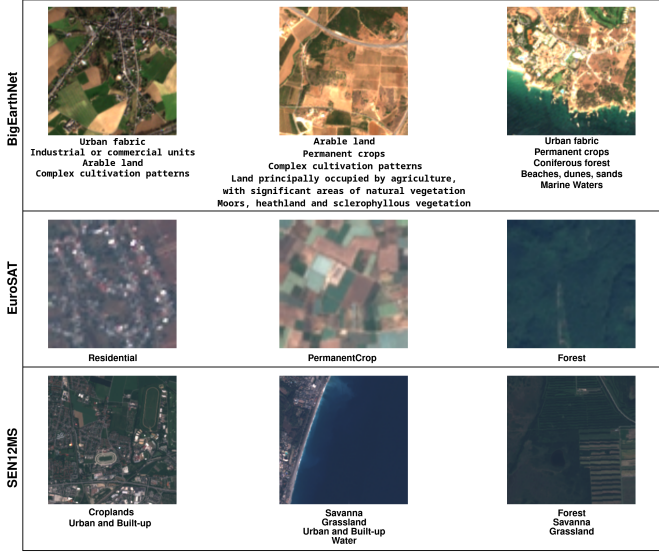


Fig. 3: Comparison of image-label pairs, sampled from the satellite datasets employed during the course of our experiments. Several innate features of the datasets, summarized in Table I, can be observed. Specifically, the effect of atmospheric corrections, which mitigate atmospheric interference thus enhancing true surface reflectance and reducing color distortion, can be highlighted when comparing BigEarthNet with EuroSAT and SEN12MS datasets. Moreover the spatial resolution differences are evident, as well as the variance with regards to the level of nomenclature detail used.

candidate captions for each class, followed by the averaging of their representations prior to computing similarities.

Models. During the course of our experiments, we employ CLIP [14] pre-trained vision transformer (ViT) models [88]. We deliberately disregarded the ResNet-based models, in favor of the ViT-based models, predicated on prior research indicating that ResNets are more susceptible to catastrophic forgetting [68], [89], while such interpolated networks suffer from variance collapse [90]. For the satellite modality encoder we utilize the SSL4EO-S12 [91] ViT-S-16 model architecture and weights, pre-trained via self-supervision using MoCo-v3 [92].

Fine-tuning on patching task. We fine-tune CLIP, as shown in Fig. 1, using RGB composites from the BigEarthNet-S2 dataset, with a batch size of 128 for 1 epoch using learning rate $1e-5$ with 200 warm-up steps with a cosine annealing learning rate schedule and the AdamW optimizer [93], [94] with weight decay [95] of 0.5. Additionally, we randomly apply ColorJitter, RandomGrayScale and GaussianBlur as data augmentations, aiming to compensate for the color variability between true-color images of surface reflectance and top-of-the-atmosphere reflectance products. During fine-tuning, we use CLIP’s text tower output, as the frozen final classification layer, so that we do not introduce any additional learnable parameters.

Cross-modal alignment. For the cross-modal alignment stage, we use a teacher-student framework, to align a pre-trained satellite (Sentinel-2) encoder with the CLIP image

Algorithm 1: Cross-modal alignment method.

Input: Pre-trained CLIP model \mathcal{M} and tokenizer \mathcal{T}
Input: Dataset $D = \{(x_i, y_i)\}_{i=1}^n, D_{classnames}, D_{prompts}\}$
Input: Pre-trained satellite modality encoder \mathcal{M}_{sat}

Output: Aligned satellite encoder \mathcal{M}_{sat}

```

/* Create classification head. */
1 Function cls_head():
2   set  $\mathcal{M}$  in inference mode
3    $W_{cls} \leftarrow []$ 
4   for  $cls \in D_{classnames}$  do
5      $T \leftarrow []$ 
6     for  $p \in D_{prompts}$  do
7        $T \leftarrow T \cup \{p.format(cls)\}$ 
8     end
9      $T \leftarrow \mathcal{T}(T)$  // tokenize
10     $\tilde{E} \leftarrow \mathcal{M}(T)$  // encode text
11    Normalize & average text embeddings  $\tilde{E}$ 
12     $W_{cls} \leftarrow W_{cls} \cup \tilde{E}$ 
13  end
14  Stack  $W_{cls}$ , transpose and apply logit scaling
15   $h \leftarrow \text{linear } classification\_head \text{ using } W_{cls}$ 
16  return  $h$ 
17
/* Align models  $\mathcal{M}_{teach}$  and  $\mathcal{M}_{stud}$ . */
18 Function align( $\mathcal{M}_{teach}, \mathcal{M}_{stud}$ ):
19   initialize frozen classification head  $h \leftarrow cls\_head()$ 
20   set  $\mathcal{M}_{stud}$  to trainable and freeze  $\mathcal{M}_{teach}$ 
21   for  $\{x_i, \tilde{x}_i\}, y_i \in D$  do
22     let  $x_i, \tilde{x}_i$  be the two modalities for sample  $i$ 
23      $E_i \leftarrow \mathcal{M}_{teach}(x_i)$ 
24      $\tilde{E}_i \leftarrow \mathcal{M}_{stud}(\tilde{x}_i)$ 
25      $y_{pred} \leftarrow h(\tilde{E}_i)$ 
26      $loss \leftarrow MSE(E_i, \tilde{E}_i) + \lambda \times CE(y_{pred}, y_i)$ 
27     ...
28   end
29   return  $\mathcal{M}_{stud}$ 
30
31 Function main():
32   /* Step 1: CLIP model Patching */
33   initialize CLIP model  $\mathcal{M}$  and tokenizer  $\mathcal{T}$ 
34    $clip\_visual \leftarrow \text{image encoder of } \mathcal{M}$ 
35    $clip\_visual.fc \leftarrow cls\_head()$ 
36    $W_{ft} \leftarrow \text{finetune } clip\_visual \text{ weights } W_{zs} \text{ on dataset } D$ 
37    $W_{paint} \leftarrow (1 - \alpha) \times W_{zs} + \alpha \times W_{ft}$ 
38   /* Step 2: Cross-modal alignment */
39   initialize satellite modality encoder  $\mathcal{M}_{sat}$ 
40    $clip\_visual \leftarrow clip\_visual.load(W_{paint})$ 
41    $\mathcal{M}_{sat} \leftarrow align(clip\_visual, \mathcal{M}_{sat}, D)$ 
42   return  $\mathcal{M}_{sat}$ 

```

and text encoders, where the satellite encoder is the trainable student network and CLIP is the frozen teacher network, as shown in Fig. 2. We use again CLIP’s text tower output, as a frozen final classification layer, so that we do not introduce any additional learnable parameters. We guide the student to mimic teacher features, using paired Sentinel-2 multi-spectral data and RGB composites from the BigEarthNet-S2 dataset, with a batch size of 256 for 5 epochs using learning rate $1e-4$ with 2000 warm-up steps with a cosine annealing learning rate schedule and the AdamW optimizer with weight decay of 0.01. We use the loss function listed in Eq. 1, where we empirically set $\lambda = 0.05$ in order to compensate for the difference in terms

of magnitude between the two loss terms, while also purposely prioritizing slightly the MSE term over CE for the first few epochs, as discussed in Section V.

Evaluation. We follow the setup of Radford et al. [14]. For the assessment of text-based zero-shot tasks, Mean Average Precision (mAP) and Accuracy (acc) are employed as the primary evaluation metrics, for multi-label and multi-class datasets, respectively. For each dataset, a set of pre-defined prompts for each class is utilized, as discussed in Section IV-B. In order to compute the embedding of each class, the embeddings of the pre-defined prompts are first computed using the text encoder, then they are averaged and L2-normalized. Each image is classified based on the cosine similarity of the L2-normalized image embedding with the class embeddings. For the evaluation of cross-modal retrieval tasks, we utilize Recall@K ($R@k$) as our performance metric. For two modalities, A and B , we compute $A \rightarrow B$ scores using the cosine similarity between modalities A and B and rank the top- k samples of modality B for each sample of modality A .

C. Results

The first stage of Algorithm 1 consists of patching CLIP by linearly interpolating weights (PAINT) [68]. The goal is to improve accuracy on satellite scene classification tasks where the model performs poorly (patching tasks), without degrading performance on tasks where accuracy is already adequate (supported tasks).

Fig. 4 summarizes the effect of patching using the BigEarthNet-19 dataset by highlighting the patching and supported tasks (ImageNet) performance trade-off for different mixing coefficients. We notice that the performance for both patching and supported tasks maximizes for $\alpha = 0.5$. We report in detail the patching results for all four CLIP ViT-based models for the patching task (i.e. BigEarthNet-19) and the representative supported task (i.e. ImageNet) for the different α weight interpolation coefficients in Appendix A. For completeness, we also include the zero-shot performance evaluation results of the patched models, for the different α coefficients, on a set of diverse satellite scene classification nomenclatures and datasets.

Fig. 5 compares and contrasts the pre- and post-patching performance for the patching and the representative supported tasks and the various nomenclatures and datasets across all candidate models. Best performance trade-off across patching and supported tasks is achieved using the larger ViT-L-14 and ViT-L-14-336 models. These results, are in-line with those of Ramasesh et al. [89] and Mehta et al. [96] who observed that larger models are less susceptible to catastrophic forgetting and Ilharco et al. [68] who highlighted that PAINT is more effective for larger models.

During the cross-modal alignment stage, we are distilling each one of the four CLIP ViT-based models into a pre-trained ViT-S-16 satellite (Sentinel-2) modality encoder. We summarize our results for zero-shot classification in Fig. 5. Appendix B contains more performance results per dataset and per class. When compared to both the non-patched and

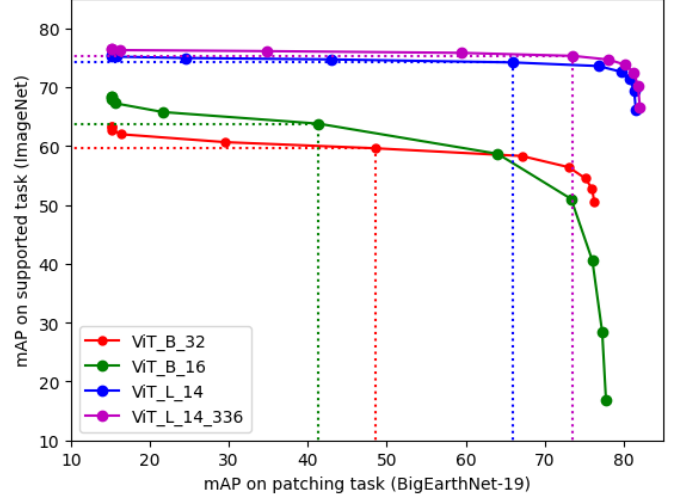


Fig. 4: Fine-tuning of CLIP ViT-based variants on BigEarthNet-19 and the interpolation of the weights of the fine-tuned and zero-shot model in order to find an intermediate solution where accuracy improves on the patching task without reducing accuracy on supported tasks. Accuracy is measured on BigEarthNet-19 as well as on ImageNet (representative supported task). Each plot shows the effect on the performance of the two tasks as α increases.

patched RGB CLIP variants, our results demonstrate notable performance improvements across all multi-spectral datasets used for evaluation, with the exception of the EuroSAT dataset. We argue that this is due to the objective function used during the alignment stage and further justify this claim in Section V. For completeness, the cross-modal retrieval results are reported in Table II, setting the baselines for the RGB \rightarrow MS and MS \rightarrow RGB retrieval tasks evaluation. It is evident that significantly better performance is achieved when using a more informative modality for the cross-modal retrieval, i.e., multi-spectral imagery aiming to retrieve the respective RGB imagery.

D. Ablation Study

In this section we systematically investigate various design choices for each one of the two stages of the proposed method. Unless explicitly stated, the experimental setup is similar to Section IV-B. We conduct the entirety of the ablation study using the smallest pre-trained CLIP model variant, namely ViT-B-32.

Patching dataset selection. The dataset used for patching is the most important parameter in the first stage of Algorithm 1. To this end, we evaluate the effect of patching CLIP and the resulting zero-shot performance, for each one of the datasets considered in Section IV-A. The experimental results stacked for each patching dataset are presented in Fig. 6. It can be observed that patching CLIP using any variation of the BigEarthNet dataset (5/19/43-class nomenclature) as the proxy task, outperforms the EuroSAT and the SEN12MS datasets in terms of both supported and patching tasks evaluation. At the same time, BigEarthNet-19 yields the best results

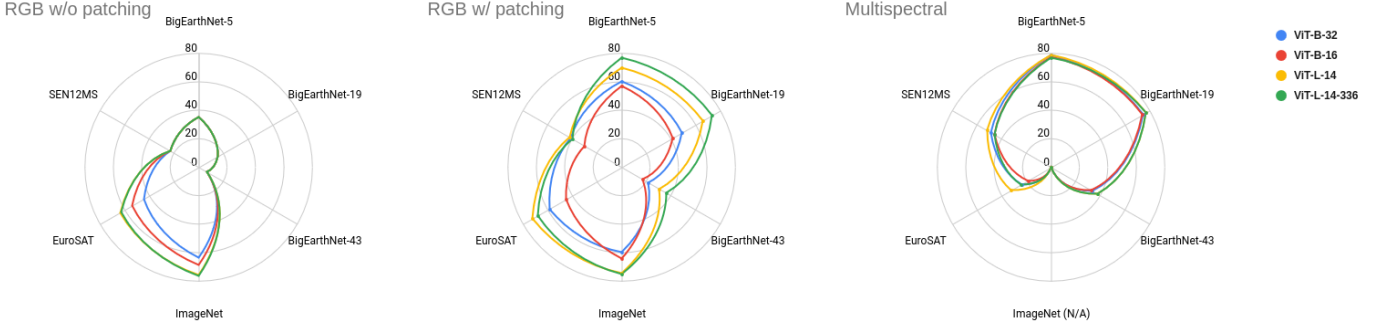


Fig. 5: Zero-shot performance on a set of diverse satellite scene classification nomenclatures and datasets. Left figure shows the performance of CLIP ViT-based variants before patching. The figure in the middle shows the performance on each dataset after patching the CLIP ViT-based encoders with BigEarthNet-19. The right figure shows the performance of the ViT-S-16 satellite encoder after the cross-modal alignment stage.

TABLE II: We evaluate the cross-modal retrieval performance of our aligned models on a set of diverse satellite imagery datasets. We present the cross-modal retrieval results for all four CLIP [14] ViT-based models, for both RGB→MS and MS→RGB retrieval.

ViT-B-32	RGB→MS				MS→RGB			
	R@1	R@5	R@10	R@20	R@1	R@5	R@10	R@20
BigEarthNet	3,61	10,61	15,86	22,90	13,44	30,44	39,95	50,35
ImageNet	–	–	–	–	–	–	–	–
EuroSAT	0,07	0,30	0,57	1,09	0,11	0,41	0,69	1,19
SEN12MS	0,31	1,34	2,42	4,07	0,31	1,40	2,55	4,08
ViT-B-16	RGB→MS				MS→RGB			
	R@1	R@5	R@10	R@20	R@1	R@5	R@10	R@20
BigEarthNet	2,81	8,60	13,16	19,42	11,21	27,14	36,67	47,57
ImageNet	–	–	–	–	–	–	–	–
EuroSAT	0,07	0,20	0,44	1,00	0,11	0,50	0,81	1,63
SEN12MS	0,26	1,09	1,85	3,24	0,47	1,78	3,06	4,88
ViT-L-14	RGB→MS				MS→RGB			
	R@1	R@5	R@10	R@20	R@1	R@5	R@10	R@20
BigEarthNet	6,84	17,93	25,03	33,75	22,78	44,26	53,87	63,43
ImageNet	–	–	–	–	–	–	–	–
EuroSAT	0,11	0,30	0,59	1,17	0,13	0,81	1,52	2,41
SEN12MS	0,28	1,20	2,22	3,96	0,93	3,65	6,13	9,76
ViT-L-14-336	RGB→MS				MS→RGB			
	R@1	R@5	R@10	R@20	R@1	R@5	R@10	R@20
BigEarthNet	7,61	19,45	26,96	35,97	23,09	44,89	54,73	64,42
ImageNet	–	–	–	–	–	–	–	–
EuroSAT	0,02	0,17	0,26	0,54	0,17	0,72	1,31	2,56
SEN12MS	0,11	0,57	1,15	2,05	0,47	2,12	3,84	6,55

among the alternative BigEarthNet class nomenclatures. The impact on the performance of the representative supported task (i.e ImageNet) is negligible among the patching datasets. More specifically, EuroSAT and BigEarthNet-43 resulting in the upper and lower performance bounds, respectively, with the rest of the datasets translating into marginal performance differences in between them.

Alignment loss variants. The alignment across all modalities can be measured using cross-modal retrieval and text-based zero-shot tasks. To that end, we evaluate the effectiveness of various alignment loss variants on the cross-modal alignment. To cover every aspect, we also evaluate the ability

of the patched CLIP model, as the teacher network during the satellite modality encoder alignment stage. We summarize our results in Table III and Table IV for classification and retrieval tasks respectively.

The results demonstrate both the necessity and the effectiveness of the initial patching stage. More specifically, we notice significant performance gains on the derived cross-modal alignment when using the patched CLIP model, for the alignment of the satellite modality encoder, instead of the original CLIP model weights. This can be observed both in the classification task (see Table III) and the retrieval task (see Table IV). In terms of the loss variants evaluated, we

TABLE III: Ablation study results, concerning the effectiveness of various alignment loss variants on the classification task. The left side of the table shows performance without patching (with the BigEarthNet-19 dataset) while the right side includes patching. The CE loss yields better results on the classification task.

Classification	Non patched			Patched		
	CE	MSE	MSE & CE	CE	MSE	MSE & CE
BigEarthNet-5	74,07	35,16	70,27	74,17	62,86	78,72
BigEarthNet-19	81,39	15,18	67,81	81,38	51,06	74,58
BigEarthNet-43	33,49	6,82	29,09	33,49	22,5	33,03
ImageNet	—	—	—	—	—	—
EuroSAT	20,13	20,28	22,83	20,37	20,57	23,75
SEN12MS	46,45	22,83	41,39	46,45	41,66	49,06

TABLE IV: The cross-modal retrieval results for all four CLIP ViT-based models, for both RGB→MS and MS→RGB retrieval. Metric used is R@5. The left side of table shows performance for different loss functions without patching while the right side shows performance with patching. The results highlight the importance of the patching stage. Additionally, the MSE loss during alignment yields better results in the retrieval tasks.

Retrieval	Non patched						Patched					
	CE		MSE		MSE & CE		CE		MSE		MSE & CE	
	RGB→MS	MS→RGB	RGB→MS	MS→RGB	RGB→MS	MS→RGB	RGB→MS	MS→RGB	RGB→MS	MS→RGB	RGB→MS	MS→RGB
BigEarthNet	0,02	0,01	8,13	28,72	5,15	19,03	0,14	0,02	17,72	45,26	10,61	30,44
ImageNet	—	—	—	—	—	—	—	—	—	—	—	—
EuroSAT	0,22	0,13	0,22	0,44	0,22	0,37	0,09	0,17	0,33	0,69	0,30	0,41
SEN12MS	0,07	0,07	1,00	1,79	1,15	1,52	0,14	0,09	1,81	2,39	1,34	1,40

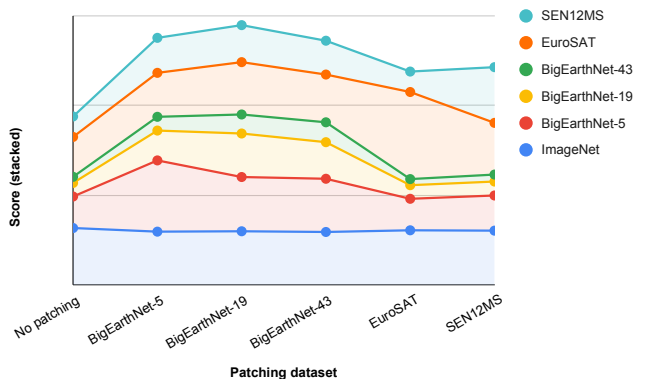


Fig. 6: Patching dataset selection ablation study. We evaluate the effect of patching CLIP and the resulting zero-shot performance, for each one of the datasets considered in Section IV-A.

yield the best results for both classification and retrieval tasks, using the proposed loss of Eq. 1. The exclusive utilization of either cross entropy (CE) or mean squared error (MSE) loss, for the satellite modality encoder alignment, results in a tendency for alignment with either the CLIP text or image encoder. More specifically, the aligned satellite modality encoder gravitates towards the CLIP text encoder when using the CE loss and towards the CLIP image encoder when using the MSE loss. This behavior disrupts the alignment between the satellite modality encoder and the residual modality.

V. DISCUSSION AND CONCLUSION

We present a straightforward method aiming to create a joint embedding space for distinct RS imagery modalities.

Our proposed method, leverages CLIP large scale pre-training, working towards a RS Vision-Language model (VLM), without relying on textual descriptions, without training from scratch, without introducing any task-specific parameters and without catastrophic forgetting. We enable, in a computationally efficient manner, a rich set of multi-modal tasks across different modalities and set preliminary baselines for cross-modal retrieval and text-based zero-shot tasks using RS imagery. We aspire for our method to serve as a stepping stone for the EO community and facilitate novel applications on RS imagery.

A. A blueprint towards satellite vision-language models

We view our proposed methodology as a blueprint for the resource-efficient development of a RS Vision-Language model (VLM). Our experimental results highlight two major challenges that warrant further attention: the generalizability of our generated VLM and the need for a clearer understanding of state-of-the-art VLMs in comparison to well-established standards and benchmarks.

In the pursuit of enhancing the generalizability of our method, it becomes essential to explore specific considerations and refinements that transcend the immediate scope of our experimental setup. We deliberately patch CLIP using a single proxy dataset, as shown in Fig. 1. Nevertheless, it should be obvious that it is extremely difficult for a single dataset to address multiple training objectives (i.e multi-class vs multi-label classification), as well as the unique challenges posed by remote sensing imagery in terms of spatial coverage, atmospheric conditions, varying perspectives, temporal and spatial resolution, which can significantly impact the performance of DL models. We summarize the characteristics of

the datasets used during the course of our experiments, in Table I. For completeness, we also provide a direct comparison of per dataset sampled image-label pairs in Fig. 3, where several differences become apparent, such as: i) the spatial resolution differences, ii) the diversity with regards to the level of nomenclature detail used, as well as iii) the effect of atmospheric corrections which in the case of BigEarthNet mitigate atmospheric interference thus enhancing true surface reflectance and reducing color distortion. A straightforward modification to the CLIP model patching method tailored on multiple datasets [68], should remedy the shortcomings observed in our experimental outcomes. Such a modification is expected to significantly improve the performance of patched models, thereby leading also to notable improvements at the cross-modal alignment stage.

A similar modification could be also introduced to our cross-modal alignment stage, seen in Fig. 2. We are confident that such a modification, would substantially improve our experimental results, summarized in Fig. 4 and Table II. Especially for multi-class classification tasks, such as EuroSAT, where our results are currently lacking in terms of performance, since this stems from our current way of aligning the Self-supervised Learning (SSL) pre-trained satellite encoder using solely the BigEarthNet dataset and as a consequence a multi-label optimization objective for the label loss part of our proposed loss function Eq. 1. Another possible improvement could also be the use of a larger SSL pre-trained satellite modality encoder. As of today, Wang et al. [91] have published a series of pre-trained Sentinel-2 encoder weights, featuring different SSL methods, yet only for ViT-S-16 architecture. This could possibly pose a limiting factor for our cross-modal alignment outcome, since it might outstrip the capacity of our aligned encoder to acquire concepts, especially when the knowledge is transferred from considerably larger CLIP encoders.

Turning our attention to benchmarking, a comprehensive examination of our approach’s performance in comparison to established standards is essential to validate its robustness and potential applications in diverse contexts. To this end, recent works [97]–[99] have been focusing on enabling a reliable assessment of progress, in the field of EO foundation models, by fabricating EO benchmark suites alongside robust methodologies for evaluating models and reporting results. Such evaluation suites, along the one used for the evaluation of CLIP [14], could ultimately provide the community with ranked candidate CLIP models and streamline future application within the EO era.

B. Bridging modalities with distinct intrinsic features

The cross-modal alignment of complementary RS imagery modalities, beyond RGB, is very important in the context of the EO community. Working towards this end, we pinpoint a pivotal juncture for the successful outcome of our cross-modal alignment stage, specifically the information gap between heterogenous modalities [100], [101]. Prompted by prior works [102], which determined that contrastive learning preserves the gap between different modalities, we suggest an

alternative loss 1 formulated as the linear combination of Mean Squared Error (MSE) and Cross Entropy (CE) losses. Contrary to Girdhar et al. [103], which trains a joint embedding space for multiple modalities using solely image alignment, we leverage guidance from the scaled CE signal in an effort to alleviate the modality gap of RGB composites and RS imagery and allow the RS modality encoder to better align within the shared embedding space while being constrained to produce similar image embeddings, due to the MSE loss. All in all, our alignment procedure resembles a plain cross-modal knowledge distillation setup, where the knowledge distillation (KD) loss has been altered to imitate the output embeddings of the teacher network, in contrast to the softened class scores. CLIP knowledge distillation has been receiving a lot of attention lately and has already proven its capabilities on a series of works [76], [104]–[108], which aspire to exploit the large scale pre-training of CLIP in an computationally efficient and interoperable way.

ACKNOWLEDGMENT

This work has received funding from the European Union’s Horizon Europe research and innovation project ThinkingEarth under grant agreement number 101130544.

REFERENCES

- [1] G. Sumbul, A. De Wall, T. Kreuziger, F. Marcelino, H. Costa, P. Benevides, M. Caetano, B. Demir, and V. Markl, “Bigearthnet-mm: A large-scale, multimodal, multilabel benchmark archive for remote sensing image classification and retrieval [software and data sets],” *IEEE Geoscience and Remote Sensing Magazine*, vol. 9, no. 3, pp. 174–180, 2021.
- [2] Y. Wang, C. M. Albrecht, N. A. A. Braham, L. Mou, and X. X. Zhu, “Self-supervised learning in remote sensing: A review,” *IEEE Geoscience and Remote Sensing Magazine*, vol. 10, no. 4, pp. 213–247, 2022.
- [3] F. Hu, G.-S. Xia, J. Hu, and L. Zhang, “Transferring deep convolutional neural networks for the scene classification of high-resolution remote sensing imagery,” *Remote Sensing*, vol. 7, no. 11, pp. 14 680–14 707, 2015.
- [4] R. Bommasani, D. A. Hudson, E. Adeli, R. Altman, S. Arora, S. von Arx, M. S. Bernstein, J. Bohg, A. Bosselut, E. Brunskill et al., “On the opportunities and risks of foundation models,” *arXiv preprint arXiv:2108.07258*, 2021.
- [5] P. W. Koh, S. Sagawa, H. Marklund, S. M. Xie, M. Zhang, A. Balsubramani, W. Hu, M. Yasunaga, R. L. Phillips, I. Gao et al., “Wilds: A benchmark of in-the-wild distribution shifts,” in *International Conference on Machine Learning*. PMLR, 2021, pp. 5637–5664.
- [6] N. I. Bountos, I. Papoutsis, D. Michail, A. Karavias, P. Elias, and I. Parcharidis, “Hephaestus: A large scale multitask dataset towards insar understanding,” in *Proceedings of the IEEE/CVF Conference on Computer Vision and Pattern Recognition*, 2022, pp. 1453–1462.
- [7] B. Qu, X. Li, D. Tao, and X. Lu, “Deep semantic understanding of high resolution remote sensing image,” in *2016 International conference on computer, information and telecommunication systems (Cits)*. IEEE, 2016, pp. 1–5.
- [8] X. Lu, B. Wang, X. Zheng, and X. Li, “Exploring models and data for remote sensing image caption generation,” *IEEE Transactions on Geoscience and Remote Sensing*, vol. 56, no. 4, pp. 2183–2195, 2017.
- [9] Z. Yuan, W. Zhang, K. Fu, X. Li, C. Deng, H. Wang, and X. Sun, “Exploring a fine-grained multiscale method for cross-modal remote sensing image retrieval,” *IEEE Transactions on Geoscience and Remote Sensing*, vol. 60, pp. 1–19, 2022.
- [10] Y. Zhan, Z. Xiong, and Y. Yuan, “Rsvg: Exploring data and models for visual grounding on remote sensing data,” *IEEE Transactions on Geoscience and Remote Sensing*, vol. 61, pp. 1–13, 2023.
- [11] S. Shen, L. H. Li, H. Tan, M. Bansal, A. Rohrbach, K.-W. Chang, Z. Yao, and K. Keutzer, “How much can clip benefit vision-and-language tasks?” *arXiv preprint arXiv:2107.06383*, 2021.

- [12] M. Barraco, M. Cornia, S. Cascianelli, L. Baraldi, and R. Cucchiara, "The unreasonable effectiveness of clip features for image captioning: an experimental analysis," in *proceedings of the IEEE/CVF conference on computer vision and pattern recognition*, 2022, pp. 4662–4670.
- [13] W. Li, L. Zhu, L. Wen, and Y. Yang, "Decap: Decoding clip latents for zero-shot captioning via text-only training," *arXiv preprint arXiv:2303.03032*, 2023.
- [14] A. Radford, J. W. Kim, C. Hallacy, A. Ramesh, G. Goh, S. Agarwal, G. Sastry, A. Askell, P. Mishkin, J. Clark *et al.*, "Learning transferable visual models from natural language supervision," in *International conference on machine learning*. PMLR, 2021, pp. 8748–8763.
- [15] M. Wang, J. Xing, and Y. Liu, "Actionclip: A new paradigm for video action recognition," *arXiv preprint arXiv:2109.08472*, 2021.
- [16] Z. Wang, Y. Lu, Q. Li, X. Tao, Y. Guo, M. Gong, and T. Liu, "Cris: Clip-driven referring image segmentation," in *Proceedings of the IEEE/CVF conference on computer vision and pattern recognition*, 2022, pp. 11 686–11 695.
- [17] O. Patashnik, Z. Wu, E. Shechtman, D. Cohen-Or, and D. Lischinski, "Styleclip: Text-driven manipulation of stylegan imagery," in *Proceedings of the IEEE/CVF International Conference on Computer Vision*, 2021, pp. 2085–2094.
- [18] M. Cornia, L. Baraldi, G. Fiameni, and R. Cucchiara, "Universal captioner: Inducing content-style separation in vision-and-language model training," *arXiv preprint arXiv:2111.12727*, 2021.
- [19] R. Mokady, A. Hertz, and A. H. Bermano, "Clipcap: Clip prefix for image captioning," *arXiv preprint arXiv:2111.09734*, 2021.
- [20] M. Tang, Z. Wang, Z. Liu, F. Rao, D. Li, and X. Li, "Clip4caption: Clip for video caption," in *Proceedings of the 29th ACM International Conference on Multimedia*, 2021, pp. 4858–4862.
- [21] A. Ramesh, M. Pavlov, G. Goh, S. Gray, C. Voss, A. Radford, M. Chen, and I. Sutskever, "Zero-shot text-to-image generation," in *International Conference on Machine Learning*. PMLR, 2021, pp. 8821–8831.
- [22] A. Ramesh, P. Dhariwal, A. Nichol, C. Chu, and M. Chen, "Hierarchical text-conditional image generation with clip latents," *arXiv preprint arXiv:2204.06125*, vol. 1, no. 2, p. 3, 2022.
- [23] J.-B. Alayrac, J. Donahue, P. Luc, A. Miech, I. Barr, Y. Hasson, K. Lenc, A. Mensch, K. Millican, M. Reynolds *et al.*, "Flamingo: a visual language model for few-shot learning," *Advances in Neural Information Processing Systems*, vol. 35, pp. 23 716–23 736, 2022.
- [24] A. Kirillov, E. Mintun, N. Ravi, H. Mao, C. Rolland, L. Gustafson, T. Xiao, S. Whitehead, A. C. Berg, W.-Y. Lo *et al.*, "Segment anything," *arXiv preprint arXiv:2304.02643*, 2023.
- [25] G. Ilharco, M. Wortsman, R. Wightman, C. Gordon, N. Carlini, R. Taori, A. Dave, V. Shankar, H. Namkoong, J. Miller, H. Hajishirzi, A. Farhadi, and L. Schmidt, "Openclip," Jul. 2021, if you use this software, please cite it as below. [Online]. Available: <https://doi.org/10.5281/zenodo.5143773>
- [26] C. Schuhmann, R. Beaumont, R. Vencu, C. Gordon, R. Wightman, M. Cherti, T. Coombes, A. Katta, C. Mullis, M. Wortsman *et al.*, "Laion-5b: An open large-scale dataset for training next generation image-text models," *Advances in Neural Information Processing Systems*, vol. 35, pp. 25 278–25 294, 2022.
- [27] M. Cherti, R. Beaumont, R. Wightman, M. Wortsman, G. Ilharco, C. Gordon, C. Schuhmann, L. Schmidt, and J. Jitsev, "Reproducible scaling laws for contrastive language-image learning," in *Proceedings of the IEEE/CVF Conference on Computer Vision and Pattern Recognition*, 2023, pp. 2818–2829.
- [28] S. Y. Gadre, G. Ilharco, A. Fang, J. Hayase, G. Smyrnis, T. Nguyen, R. Marten, M. Wortsman, D. Ghosh, J. Zhang *et al.*, "Datacomp: In search of the next generation of multimodal datasets," *arXiv preprint arXiv:2304.14108*, 2023.
- [29] A. Fang, A. M. Jose, A. Jain, L. Schmidt, A. Toshev, and V. Shankar, "Data filtering networks," *arXiv preprint arXiv:2309.17425*, 2023.
- [30] H. Xu, S. Xie, X. E. Tan, P.-Y. Huang, R. Howes, V. Sharma, S.-W. Li, G. Ghosh, L. Zettlemoyer, and C. Feichtenhofer, "Demystifying clip data," *arXiv preprint arXiv:2309.16671*, 2023.
- [31] Q. Sun, Y. Fang, L. Wu, X. Wang, and Y. Cao, "Eva-clip: Improved training techniques for clip at scale," *arXiv preprint arXiv:2303.15389*, 2023.
- [32] X. Li, Z. Wang, and C. Xie, "An inverse scaling law for clip training," *arXiv preprint arXiv:2305.07017*, 2023.
- [33] —, "Clipa-v2: Scaling clip training with 81.1% zero-shot imagenet accuracy within a \$10,000 budget; an extra \$4,000 unlocks 81.8% accuracy," *arXiv preprint arXiv:2306.15658*, 2023.
- [34] X. Zhai, B. Mustafa, A. Kolesnikov, and L. Beyer, "Sigmoid loss for language image pre-training," in *2023 IEEE/CVF International Conference on Computer Vision (ICCV)*. Los Alamitos, CA, USA: IEEE Computer Society, oct 2023, pp. 11 941–11 952. [Online]. Available: <https://doi.ieeecomputersociety.org/10.1109/ICCV51070.2023.01100>
- [35] Z. Wang, Z. Wu, D. Agarwal, and J. Sun, "MedCLIP: Contrastive learning from unpaired medical images and text," in *Proceedings of the 2022 Conference on Empirical Methods in Natural Language Processing*, Y. Goldberg, Z. Kozareva, and Y. Zhang, Eds. Abu Dhabi, United Arab Emirates: Association for Computational Linguistics, Dec. 2022, pp. 3876–3887. [Online]. Available: <https://aclanthology.org/2022.emnlp-main.256>
- [36] S. Eslami, C. Meinel, and G. De Melo, "Pubmedclip: How much does clip benefit visual question answering in the medical domain?" in *Findings of the Association for Computational Linguistics: EACL 2023*, 2023, pp. 1151–1163.
- [37] S. Zhang, Y. Xu, N. Usuyama, J. Bagga, R. Tinn, S. Preston, R. Rao, M. Wei, N. Valluri, C. Wong *et al.*, "Large-scale domain-specific pretraining for biomedical vision-language processing," *arXiv preprint arXiv:2303.00915*, 2023.
- [38] Z. Zhao, Y. Liu, H. Wu, Y. Li, S. Wang, L. Teng, D. Liu, X. Li, Z. Cui, Q. Wang *et al.*, "Clip in medical imaging: A comprehensive survey," *arXiv preprint arXiv:2312.07353*, 2023.
- [39] O. Pelka, S. Koitka, J. Rückert, F. Nensa, and C. M. Friedrich, "Radiology objects in context (roco): a multimodal image dataset," in *Intravascular Imaging and Computer Assisted Stenting and Large-Scale Annotation of Biomedical Data and Expert Label Synthesis: 7th Joint International Workshop, CVII-STENT 2018 and Third International Workshop, LABELS 2018, Held in Conjunction with MICCAI 2018, Granada, Spain, September 16, 2018, Proceedings 3*. Springer, 2018, pp. 180–189.
- [40] S. Subramanian, L. L. Wang, S. Mehta, B. Bogin, M. van Zuylen, S. Parasa, S. Singh, M. Gardner, and H. Hajishirzi, "Medicat: A dataset of medical images, captions, and textual references," *arXiv preprint arXiv:2010.06000*, 2020.
- [41] W. Lin, Z. Zhao, X. Zhang, C. Wu, Y. Zhang, Y. Wang, and W. Xie, "Pmc-clip: Contrastive language-image pre-training using biomedical documents," *arXiv preprint arXiv:2303.07240*, 2023.
- [42] J. Liu, Z. Wang, Q. Ye, D. Chong, P. Zhou, and Y. Hua, "Qilin-med-vl: Towards chinese large vision-language model for general healthcare," *arXiv preprint arXiv:2310.17956*, 2023.
- [43] A. E. Johnson, T. J. Pollard, S. J. Berkowitz, N. R. Greenbaum, M. P. Lungren, C.-y. Deng, R. G. Mark, and S. Horng, "Mimic-cxr, a de-identified publicly available database of chest radiographs with free-text reports," *Scientific data*, vol. 6, no. 1, p. 317, 2019.
- [44] A. Bustos, A. Pertusa, J.-M. Salinas, and M. De La Iglesia-Vaya, "Padchest: A large chest x-ray image dataset with multi-label annotated reports," *Medical image analysis*, vol. 66, p. 101797, 2020.
- [45] M. Li, W. Cai, R. Liu, Y. Weng, X. Zhao, C. Wang, X. Chen, Z. Liu, C. Pan, M. Li *et al.*, "Ffa-ir: Towards an explainable and reliable medical report generation benchmark," in *Thirty-fifth Conference on Neural Information Processing Systems Datasets and Benchmarks Track (Round 2)*, 2021.
- [46] Z. Huang, F. Bianchi, M. Yuksekgonul, T. J. Montine, and J. Zou, "A visual-language foundation model for pathology image analysis using medical twitter," *Nature medicine*, vol. 29, no. 9, pp. 2307–2316, 2023.
- [47] W. O. Ikezogwo, M. S. Seyfioglu, F. Ghezloo, D. S. C. Geva, F. S. Mohammed, P. K. Anand, R. Krishna, and L. Shapiro, "Quilt-1m: One million image-text pairs for histopathology," *arXiv preprint arXiv:2306.11207*, 2023.
- [48] A. Arutiunian, D. Vidhani, G. Venkatesh, M. Bhaskar, R. Ghosh, and S. Pal, "Fine tuning clip with remote sensing (satellite) images and captions," 2021.
- [49] M. Czerwinski, R. Atkinson, and C. Tachtatzis, "Detecting cloud presence in satellite images using the rgb-based clip vision-language model," in *International Geoscience and Remote Sensing Symposium*, 2023.
- [50] M. Singha, A. Jha, B. Solanki, S. Bose, and B. Banerjee, "Applenet: Visual attention parameterized prompt learning for few-shot remote sensing image generalization using clip," in *Proceedings of the IEEE/CVF Conference on Computer Vision and Pattern Recognition*, 2023.
- [51] F. Liu, D. Chen, Z. Guan, X. Zhou, J. Zhu, and J. Zhou, "Remotecclip: A vision language foundation model for remote sensing," *arXiv preprint arXiv:2306.11029*, 2023.
- [52] Z. Zhang, T. Zhao, Y. Guo, and J. Yin, "Rs5m: A large scale vision-language dataset for remote sensing vision-language foundation model," *arXiv preprint arXiv:2306.11300*, 2023.

- [53] Y. Yuan, Y. Zhan, and Z. Xiong, "Parameter-efficient transfer learning for remote sensing image-text retrieval," *IEEE Transactions on Geoscience and Remote Sensing*, 2023.
- [54] N. Houlsby, A. Giurgiu, S. Jastrzebski, B. Morrone, Q. De Laroussilhe, A. Gesmundo, M. Attariyan, and S. Gelly, "Parameter-efficient transfer learning for nlp," in *International Conference on Machine Learning*, PMLR, 2019, pp. 2790–2799.
- [55] S. Mo, M. Kim, K. Lee, and J. Shin, "S-clip: Semi-supervised vision-language learning using few specialist captions," in *Thirty-seventh Conference on Neural Information Processing Systems*, 2023.
- [56] A. Bhattacharya, M. Singha, A. Jha, and B. Banerjee, "C-saw: Self-supervised prompt learning for image generalization in remote sensing," *arXiv preprint arXiv:2311.15812*, 2023.
- [57] A. Dhakal, A. Ahmad, S. Khanal, S. Sastry, and N. Jacobs, "Sat2cap: Mapping fine-grained textual descriptions from satellite images," *arXiv preprint arXiv:2307.15904*, 2023.
- [58] U. Mall, C. P. Phoo, M. K. Liu, C. Vondrick, B. Hariharan, and K. Bala, "Remote sensing vision-language foundation models without annotations via ground remote alignment," *arXiv preprint arXiv:2312.06960*, 2023.
- [59] E. Rolf, K. Klemmer, C. Robinson, and H. Kerner, "Mission critical-satellite data is a distinct modality in machine learning," *arXiv preprint arXiv:2402.01444*, 2024.
- [60] J. Li, D. Hong, L. Gao, J. Yao, K. Zheng, B. Zhang, and J. Chanussot, "Deep learning in multimodal remote sensing data fusion: A comprehensive review," *International Journal of Applied Earth Observation and Geoinformation*, vol. 112, p. 102926, 2022.
- [61] Z. Zhang, G. Vosselman, M. Gerke, D. Tuia, and M. Y. Yang, "Change detection between multimodal remote sensing data using siamese cnn," 2018.
- [62] B. Uzkent, E. Sheehan, C. Meng, Z. Tang, M. Burke, D. Lobell, and S. Ermon, "Learning to interpret satellite images in global scale using wikipedia," *arXiv preprint arXiv:1905.02506*, 2019.
- [63] A. Toker, Q. Zhou, M. Maximov, and L. Leal-Taixé, "Coming down to earth: Satellite-to-street view synthesis for geo-localization," in *Proceedings of the IEEE/CVF Conference on Computer Vision and Pattern Recognition*, 2021, pp. 6488–6497.
- [64] M. Allen, F. Dorr, J. A. Gallego-Mejia, L. Martínez-Ferrer, A. Jungbluth, F. Kalaitzis, and R. Ramos-Pollán, "Fewshot learning on global multimodal embeddings for earth observation tasks," *arXiv preprint arXiv:2310.00119*, 2023.
- [65] K. Klemmer, E. Rolf, C. Robinson, L. Mackey, and M. Rußwurm, "Satclip: Global, general-purpose location embeddings with satellite imagery," *arXiv preprint arXiv:2311.17179*, 2023.
- [66] V. V. Cepeda, G. K. Nayak, and M. Shah, "Geoclip: Clip-inspired alignment between locations and images for effective worldwide geo-localization," *arXiv preprint arXiv:2309.16020*, 2023.
- [67] S. Khanal, S. Sastry, A. Dhakal, and N. Jacobs, "Learning tri-modal embeddings for zero-shot soundscape mapping," *arXiv preprint arXiv:2309.10667*, 2023.
- [68] G. Ilharco, M. Wortsman, S. Y. Gadre, S. Song, H. Hajishirzi, S. Kornblith, A. Farhadi, and L. Schmidt, "Patching open-vocabulary models by interpolating weights," *Advances in Neural Information Processing Systems*, vol. 35, pp. 29 262–29 277, 2022.
- [69] C. Jia, Y. Yang, Y. Xia, Y.-T. Chen, Z. Parekh, H. Pham, Q. Le, Y.-H. Sung, Z. Li, and T. Duerig, "Scaling up visual and vision-language representation learning with noisy text supervision," in *International conference on machine learning*. PMLR, 2021, pp. 4904–4916.
- [70] H. Pham, Z. Dai, G. Ghiasi, K. Kawaguchi, H. Liu, A. W. Yu, J. Yu, Y.-T. Chen, M.-T. Luong, Y. Wu *et al.*, "Combined scaling for zero-shot transfer learning," *Neurocomputing*, vol. 555, p. 126658, 2023.
- [71] J. Kirkpatrick, R. Pascanu, N. Rabinowitz, J. Veness, G. Desjardins, A. A. Rusu, K. Milan, J. Quan, T. Ramalho, A. Grabska-Barwinska *et al.*, "Overcoming catastrophic forgetting in neural networks," *Proceedings of the national academy of sciences*, vol. 114, no. 13, pp. 3521–3526, 2017.
- [72] G. Hinton, O. Vinyals, and J. Dean, "Distilling the knowledge in a neural network," *arXiv preprint arXiv:1503.02531*, 2015.
- [73] Z. Fang, J. Wang, X. Hu, L. Wang, Y. Yang, and Z. Liu, "Compressing visual-linguistic model via knowledge distillation," in *Proceedings of the IEEE/CVF International Conference on Computer Vision*, 2021, pp. 1428–1438.
- [74] J. Yang, B. Martinez, A. Bulat, and G. Tzimiropoulos, "Knowledge distillation via softmax regression representation learning," in *International Conference on Learning Representations*, 2020.
- [75] T. Kim, J. Oh, N. Kim, S. Cho, and S.-Y. Yun, "Comparing kullback-leibler divergence and mean squared error loss in knowledge distillation," *arXiv preprint arXiv:2105.08919*, 2021.
- [76] C. Yang, Z. An, L. Huang, J. Bi, X. Yu, H. Yang, and Y. Xu, "Clip-kd: An empirical study of distilling clip models," 2023.
- [77] G. Sumbul, M. Charfuelan, B. Demir, and V. Markl, "Bigearthnet: A large-scale benchmark archive for remote sensing image understanding," in *IGARSS 2019-2019 IEEE International Geoscience and Remote Sensing Symposium*. IEEE, 2019, pp. 5901–5904.
- [78] Copernicus. (2018) Corine land cover 2018. [Online]. Available: <https://land.copernicus.eu/pan-european/corine-land-cover/clc2018>
- [79] G. Sumbul, J. Kang, T. Kreuziger, F. Marcelino, H. Costa, P. Benevides, M. Caetano, and B. Demir, "Bigearthnet dataset with a new nomenclature for remote sensing image understanding," 2020.
- [80] P. Helber, B. Bischke, A. Dengel, and D. Borth, "Eurosat: A novel dataset and deep learning benchmark for land use and land cover classification," *IEEE Journal of Selected Topics in Applied Earth Observations and Remote Sensing*, 2019.
- [81] M. Schmitt, L. H. Hughes, C. Qiu, and X. X. Zhu, "Sen12ms – a curated dataset of georeferenced multi-spectral sentinel-1/2 imagery for deep learning and data fusion," in *ISPRS Annals of the Photogrammetry, Remote Sensing and Spatial Information Sciences*, vol. IV-2/W7, 2019, pp. 153–160.
- [82] T. R. Loveland and A. Belward, "The international geosphere biosphere programme data and information system global land cover data set (discover)," *Acta Astronautica*, vol. 41, no. 4-10, pp. 681–689, 1997.
- [83] A. Di Gregorio, *Land cover classification system: classification concepts and user manual: LCCS*. Food & Agriculture Org., 2005, vol. 2.
- [84] M. Schmitt and Y.-L. Wu, "Remote sensing image classification with the sen12ms dataset," in *ISPRS Annals of the Photogrammetry, Remote Sensing and Spatial Information Sciences*, vol. V-2-2021, 2021, pp. 101–106.
- [85] N. Yokoya, P. Ghamisi, R. Hansch, and M. Schmitt, "Report on the 2020 ieee grss data fusion contest-global land cover mapping with weak supervision [technical committees]," *IEEE Geoscience and Remote Sensing Magazine*, vol. 8, no. 4, pp. 134–137, 2020.
- [86] J. Deng, W. Dong, R. Socher, L.-J. Li, K. Li, and L. Fei-Fei, "Imagenet: A large-scale hierarchical image database," in *2009 IEEE conference on computer vision and pattern recognition*. Ieee, 2009, pp. 248–255.
- [87] X. Zhai, X. Wang, B. Mustafa, A. Steiner, D. Keysers, A. Kolesnikov, and L. Beyer, "Lit: Zero-shot transfer with locked-image text tuning," in *Proceedings of the IEEE/CVF Conference on Computer Vision and Pattern Recognition*, 2022, pp. 18 123–18 133.
- [88] A. Dosovitskiy, L. Beyer, A. Kolesnikov, D. Weissenborn, X. Zhai, T. Unterthiner, M. Dehghani, M. Minderer, G. Heigold, S. Gelly *et al.*, "An image is worth 16x16 words: Transformers for image recognition at scale," *arXiv preprint arXiv:2010.11929*, 2020.
- [89] V. V. Ramasesh, A. Lewkowycz, and E. Dyer, "Effect of scale on catastrophic forgetting in neural networks," in *International Conference on Learning Representations*, 2021.
- [90] K. Jordan, H. Sedghi, O. Saukh, R. Entezari, and B. Neyshabur, "Repair: Renormalizing permuted activations for interpolation repair," *arXiv preprint arXiv:2211.08403*, 2022.
- [91] Y. Wang, N. A. A. Braham, Z. Xiong, C. Liu, C. M. Albrecht, and X. X. Zhu, "Ssl4eo-s12: A large-scale multi-modal, multi-temporal dataset for self-supervised learning in earth observation," *arXiv preprint arXiv:2211.07044*, 2022.
- [92] X. Chen, S. Xie, and K. He, "An empirical study of training self-supervised vision transformers," in *2021 IEEE/CVF International Conference on Computer Vision (ICCV)*. Los Alamitos, CA, USA: IEEE Computer Society, oct 2021, pp. 9620–9629. [Online]. Available: <https://doi.ieeecomputersociety.org/10.1109/ICCV48922.2021.00950>
- [93] D. P. Kingma and J. Ba, "Adam: A method for stochastic optimization," *arXiv preprint arXiv:1412.6980*, 2014.
- [94] I. Loshchilov and F. Hutter, "Decoupled weight decay regularization," *arXiv preprint arXiv:1711.05101*, 2017.
- [95] M. Andriushchenko, F. D'Angelo, A. Varre, and N. Flammarion, "Why do we need weight decay in modern deep learning?" 2023.
- [96] S. V. Mehta, D. Patil, S. Chandar, and E. Strubell, "An empirical investigation of the role of pre-training in lifelong learning," *Journal of Machine Learning Research*, vol. 24, no. 214, pp. 1–50, 2023.
- [97] J. Roberts, K. Han, and S. Albanie, "Satin: A multi-task metadataset for classifying satellite imagery using vision-language models," *arXiv preprint arXiv:2304.11619*, 2023.
- [98] A. Lacoste, N. Lehmann, P. Rodriguez, E. D. Sherwin, H. Kerner, B. Lütjens, J. A. Irvin, D. Dao, H. Alemohammad, A. Drouin *et al.*,

- “Geo-bench: Toward foundation models for earth monitoring,” *arXiv preprint arXiv:2306.03831*, 2023.
- [99] N. I. Bountos, A. Ouaknine, and D. Rolnick, “Fomo-bench: a multi-modal, multi-scale and multi-task forest monitoring benchmark for remote sensing foundation models,” *arXiv preprint arXiv:2312.10114*, 2023.
- [100] P. Shi, M. C. Welle, M. Björkman, and D. Kragic, “Towards understanding the modality gap in clip,” in *ICLR 2023 Workshop on Multimodal Representation Learning: Perks and Pitfalls*, 2023.
- [101] H. Fu, R. Wu, C. Liu, and J. Sun, “Mcen: Bridging cross-modal gap between cooking recipes and dish images with latent variable model,” in *Proceedings of the IEEE/CVF Conference on Computer Vision and Pattern Recognition*, 2020, pp. 14 570–14 580.
- [102] V. W. Liang, Y. Zhang, Y. Kwon, S. Yeung, and J. Y. Zou, “Mind the gap: Understanding the modality gap in multi-modal contrastive representation learning,” *Advances in Neural Information Processing Systems*, vol. 35, pp. 17 612–17 625, 2022.
- [103] R. Girdhar, A. El-Nouby, Z. Liu, M. Singh, K. V. Alwala, A. Joulin, and I. Misra, “Imagebind: One embedding space to bind them all,” in *Proceedings of the IEEE/CVF Conference on Computer Vision and Pattern Recognition*, 2023, pp. 15 180–15 190.
- [104] K. Wu, H. Peng, Z. Zhou, B. Xiao, M. Liu, L. Yuan, H. Xuan, M. Valenzuela, X. S. Chen, X. Wang *et al.*, “Tinyclip: Clip distillation via affinity mimicking and weight inheritance,” in *Proceedings of the IEEE/CVF International Conference on Computer Vision*, 2023, pp. 21 970–21 980.
- [105] R. Pei, J. Liu, W. Li, B. Shao, S. Xu, P. Dai, J. Lu, and Y. Yan, “Clipping: Distilling clip-based models with a student base for video-language retrieval,” in *Proceedings of the IEEE/CVF Conference on Computer Vision and Pattern Recognition*, 2023, pp. 18 983–18 992.
- [106] Z. Wang, N. Codella, Y.-C. Chen, L. Zhou, J. Yang, X. Dai, B. Xiao, H. You, S.-F. Chang, and L. Yuan, “Clip-td: Clip targeted distillation for vision-language tasks,” *arXiv preprint arXiv:2201.05729*, 2022.
- [107] H.-H. Wu, P. Seetharaman, K. Kumar, and J. P. Bello, “Wav2clip: Learning robust audio representations from clip,” in *ICASSP 2022-2022 IEEE International Conference on Acoustics, Speech and Signal Processing (ICASSP)*. IEEE, 2022, pp. 4563–4567.
- [108] A. Guzhov, F. Raue, J. Hees, and A. Dengel, “Audioclip: Extending clip to image, text and audio,” in *ICASSP 2022-2022 IEEE International Conference on Acoustics, Speech and Signal Processing (ICASSP)*. IEEE, 2022, pp. 976–980.

APPENDIX A

PATCHED MODELS ZERO-SHOT PERFORMANCE

In this section we report in detail the patching results for all four CLIP ViT-based models for the patching task (i.e. BigEarthNet-19) and the representative supported task (i.e. ImageNet) for the different α weight interpolation coefficients. For completeness, we also include the zero-shot performance evaluation results of the patched models, for the different α coefficients, on a set of diverse satellite scene classification nomenclatures and datasets. See Table V.

APPENDIX B

PER-CLASS PERFORMANCE

In this section we present the per-class performance of our best CLIP-L-14 model. As always we present the performance of the model pre- and post-patching with BigEarthNet-19. Additionally the plots contain the performance of the ViT-S-16 after alignment with the CLIP-L-14 model. Figures 7 and 8 present per-class performance on BigEarthNet-5 and BigEarthNet-19 respectively, while Figure 9 present per-class performance on BigEarthNet-43. Finally, Figures 10 and 11 contain per-class performance on SEN12MS and EuroSAT.

In the case of SEN12MS, we replicated the experimental setup reported by the authors and used their published PyTorch checkpoints in order to calculate mAP for their SOTA

ResNet50 model and provide a fair comparison with our results. Unfortunately, there were no publicly available PyTorch checkpoints for EuroSAT and BigEarthNet, to evaluate per class performance.

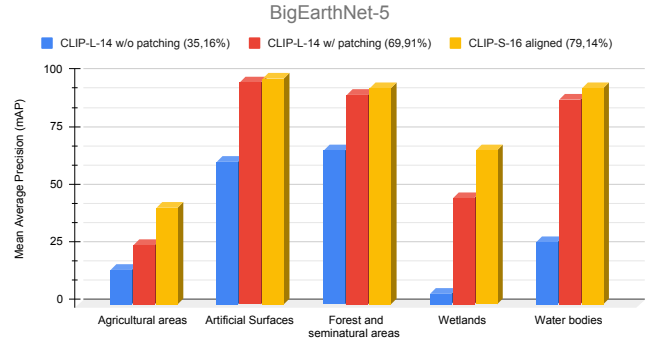


Fig. 7: Zero-shot performance comparison of our best performing CLIP-L-14 model on BigEarthNet-43 RGB, pre- and post-patching on BigEarthNet-19 RGB. Additionally, performance of the pre-trained ViT-S-16 after alignment with the patched CLIP-L-14 model. BigEarthNet-5 features a much simpler 5-class nomenclature, in comparison to the BigEarthNet-19 19-class one.

TABLE V: We evaluate the zero-shot performance of the patched models on a set of diverse satellite scene classification nomenclatures and datasets. We consider BigEarthNet-19 as a proxy dataset for the satellite scene classification task, and ImageNet as a representative supported task. We present the patching results for all four CLIP [14] ViT-based models, in conjunction with the different α weight interpolation values.

ViT-B-32	α										
	0,00	0,10	0,20	0,30	0,40	0,50	0,60	0,70	0,80	0,90	1,00
BigEarthNet-19 (mAP)	15,18	15,18	15,18	16,38	29,55	48,58	67,1	73,04	75,15	76,01	76,28
ImageNet (acc)	63,25	63,29	62,78	62,0	60,66	59,62	58,31	56,41	54,51	52,73	50,45
EuroSAT (acc)	44,53	50,59	55,52	57,81	58,54	58,42	54,69	48,48	39,49	28,39	17,2
SEN12MS (mAP)	22,83	22,83	22,83	22,84	30,46	41,32	47,85	50,23	50,29	50,14	50,06
BigEarthNet-5 (mAP)	35,16	35,16	35,16	37,74	52,29	60,56	68,04	69,10	69,20	69,48	69,62
BigEarthNet-43 (mAP)	6,82	6,82	6,82	7,57	13,11	21,24	29,43	32,36	33,15	33,28	33,14

ViT-B-16	α										
	0,00	0,10	0,20	0,30	0,40	0,50	0,60	0,70	0,80	0,90	1,00
BigEarthNet-19 (mAP)	15,18	15,18	15,18	15,59	21,62	41,37	64,05	73,35	76,04	77,28	77,76
ImageNet (acc)	68,38	68,3	67,92	67,27	65,78	63,8	58,68	51,01	40,54	28,45	16,88
EuroSAT (acc)	53,76	55,72	55,79	53,54	50,47	45,12	37,62	39,65	41,76	41,99	40,42
SEN12MS (mAP)	22,83	22,83	22,83	22,83	23,84	30,03	38,52	45,24	46,10	44,91	43,82
BigEarthNet-5 (mAP)	35,16	35,16	35,16	35,88	45,13	56,79	67,07	73,86	74,46	74,04	73,62
BigEarthNet-43 (mAP)	6,82	6,82	6,82	7,10	9,73	16,72	26,65	31,55	32,36	32,52	32,48

ViT-L-14	α										
	0,00	0,10	0,20	0,30	0,40	0,50	0,60	0,70	0,80	0,90	1,00
BigEarthNet-19 (mAP)	15,18	15,2	15,75	24,5	42,93	65,92	76,84	79,66	80,78	81,33	81,54
ImageNet (acc)	75,49	75,33	75,19	74,96	74,72	74,21	73,59	72,62	71,36	69,37	66,24
EuroSAT (acc)	63,72	69,0	70,96	72,05	72,27	72,25	72,04	71,36	69,81	67,35	64,15
SEN12MS (mAP)	22,83	22,83	22,87	24,79	34,17	42,03	48,43	51,19	51,04	50,44	50,06
BigEarthNet-5 (mAP)	35,16	35,17	35,74	50,59	58,86	69,90	76,72	77,14	76,55	76,15	75,97
BigEarthNet-43 (mAP)	6,83	6,83	7,06	10,98	18,92	30,14	37,84	39,87	40,14	39,91	39,43

ViT-L-14-336	α										
	0,00	0,10	0,20	0,30	0,40	0,50	0,60	0,70	0,80	0,90	1,00
BigEarthNet-19 (mAP)	15,18	15,18	16,21	34,79	59,47	73,59	78,12	80,18	81,27	81,83	82,05
ImageNet (acc)	76,49	76,42	76,3	76,13	75,83	75,32	74,68	73,81	72,51	70,21	66,54
EuroSAT (acc)	62,88	68,11	68,89	66,23	69,07	68,2	64,83	61,97	59,78	57,52	54,82
SEN12MS (mAP)	22,83	22,83	22,83	22,98	27,98	39,75	48,33	50,50	50,49	49,72	48,85
BigEarthNet-5 (mAP)	35,16	35,16	36,05	60,25	70,59	76,95	78,68	78,82	78,88	79,05	79,23
BigEarthNet-43 (mAP)	6,82	6,82	7,12	14,96	27,45	36,01	38,64	39,38	39,50	39,40	39,13

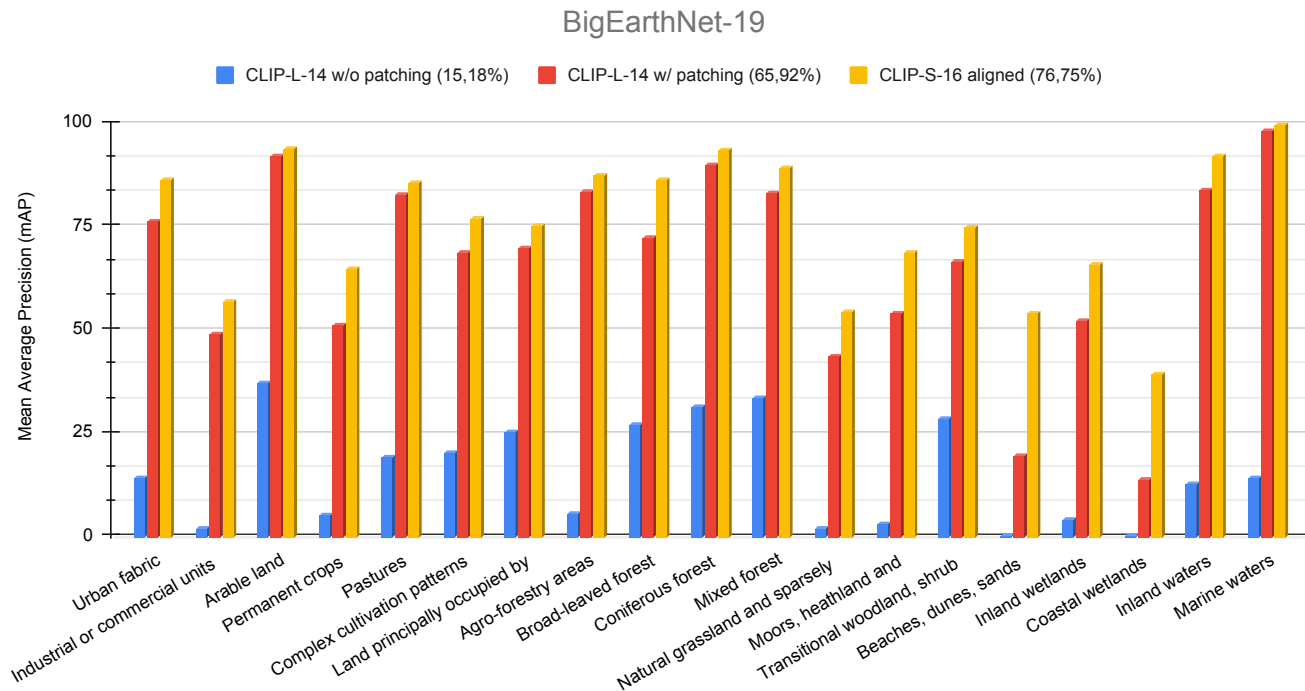


Fig. 8: Performance comparison of our best performing CLIP-L-14 model, pre- and post-patching on BigEarthNet-19 RGB. Additionally, performance of the pre-trained ViT-S-16 after alignment with the patched CLIP-L-14 model.

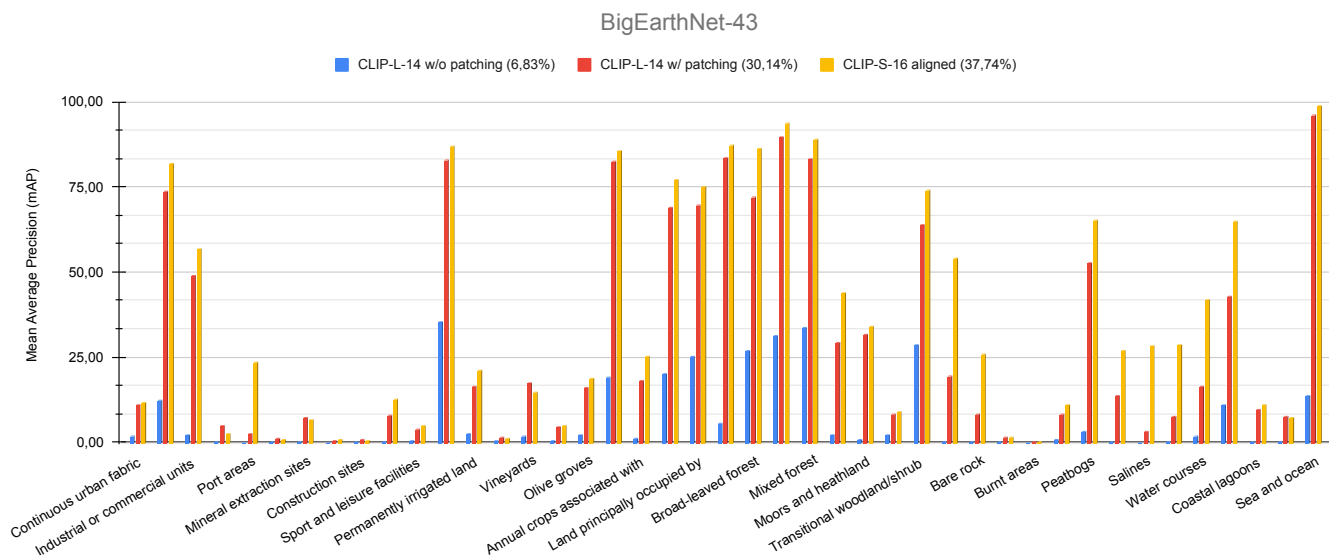


Fig. 9: Zero-shot performance comparison of our best performing CLIP-L-14 model on BigEarthNet-43 RGB, pre- and post-patching on BigEarthNet-19 RGB. Additionally, performance of the pre-trained ViT-S-16 after alignment with the patched CLIP-L-14 model. BigEarthNet-43 features a detailed 43-class nomenclature, in comparison to the BigEarthNet-19 19-class one.

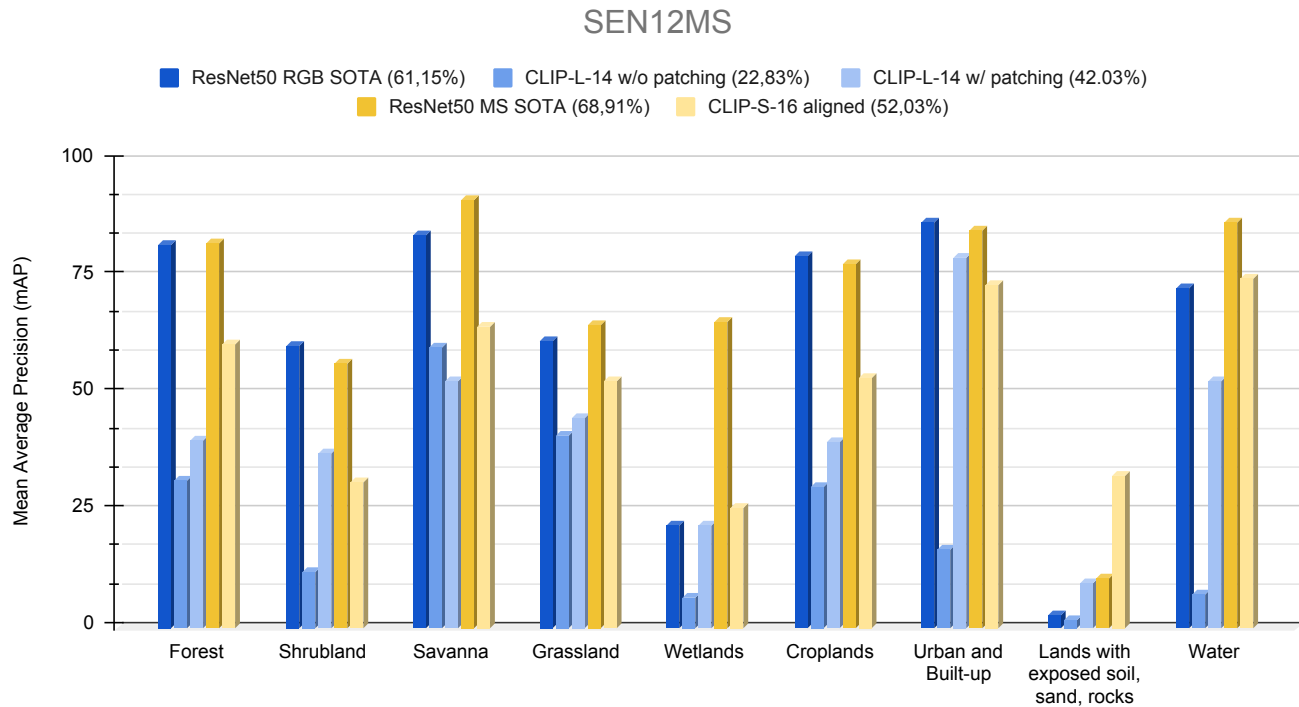


Fig. 10: Zero-shot performance comparison of our best performing CLIP-L-14 model on SEN12MS RGB, pre- and post-patching on BigEarthNet-19 RGB. Additionally, performance of the pre-trained ViT-S-16 after alignment with the patched CLIP-L-14 model. We also include the evaluation results of the ResNet50 SOTA model published by the dataset authors. SEN12MS features a 9-class nomenclature.

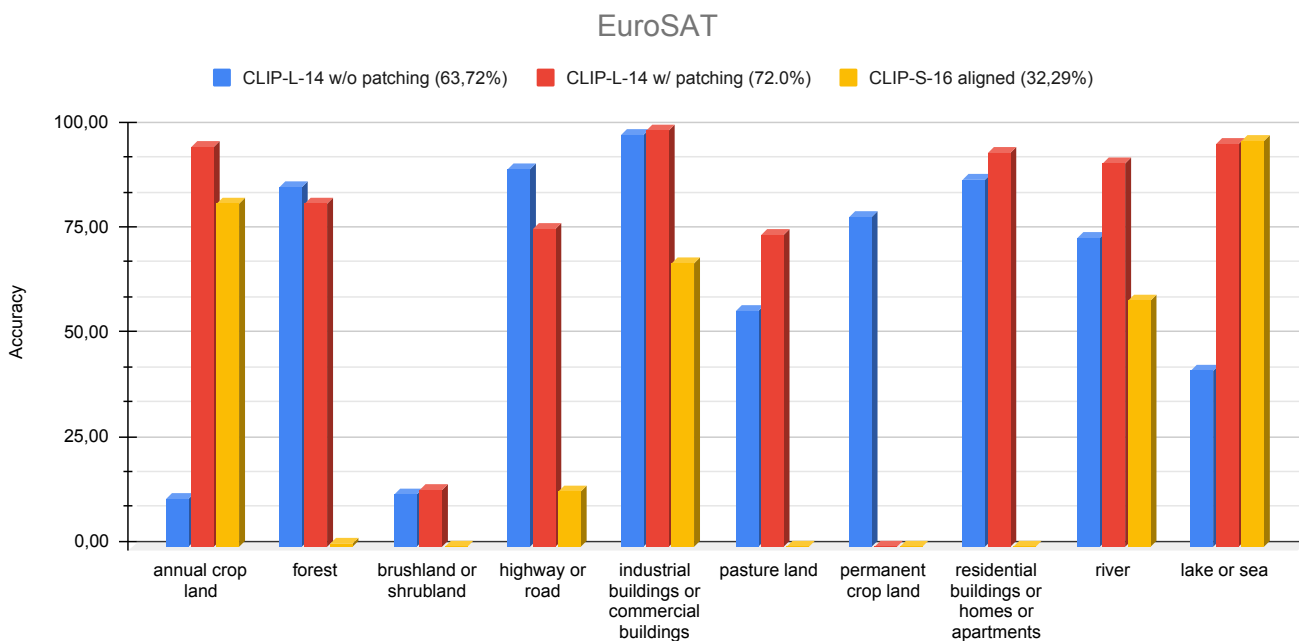


Fig. 11: Zero-shot performance comparison of our best performing CLIP-L-14 model on EuroSAT RGB, pre- and post-patching on BigEarthNet-19. Additionally, performance of the pre-trained ViT-S-16 after alignment with the patched CLIP-L-14 model. EuroSAT features a 10-class nomenclature.